FACULTY OF TECHNOLOGY

CHARACTERIZATION OF PHYSICAL AND MECHANICAL PROPERTIES OF ROCKS FROM OTANMÄKI, FINLAND

ABUBAKAR OSMANU

MINERAL RESOURCES AND SUSTAINABLE MINING
(MINING ENGINEERING AND MINERAL PROCESSING)
Master's thesis
JULY 2020

ABSTRACT

Characterization of physical and mechanical properties of rocks from Otanmäki, Finland.

Abubakar Osmanu

University of Oulu, Mineral Resources and Sustainable Mining (Mining engineering and Mineral Processing)

Master's thesis 2020, 96 pages.

Supervisor: Dr. Adeyemi Aladejare

Physical and mechanical properties of rocks are important parameters for geological engineering and design of engineering structures, be it in the civil and/or mining sector. Rock physical properties include density, porosity, etc., and Young's modulus, Poisson's ratio and rock strength include some mechanical properties of rocks. These properties can be obtained by laboratory tests. This study aims at characterizing selected rock physical and mechanical properties to assist in predicting rock mass behavior when used in engineering structures, to discuss key rock petrographical features that affect strength and compare the prediction capacities of multiple linear regression and artificial neural network (ANN) models.

The study investigates selected physical and mechanical properties from two igneous rock types, gabbro and granite, from the Otanmäki area, central Finland. The test results were used for the ANN and multiple regression models.

In the analyses, a total of 25 cases from the two rocks were tested for uniaxial compression strength (UCS), Young's modulus, Poisson's ratio, Brazilian tensile strength (BTS), density, porosity and water content. Samples were also analyzed for petrographic and chemical compositions. Results from the analyses indicate the importance of adhering to testing standards because of inconsistencies and wide variations observed between non-standardized as opposed to standardized specimens, and the need for large database for reliable predictive models. It presents ANN techniques as having a good generalization capacity for multi-variable nonlinear prediction.

key words: Uniaxial compressive strength, Brazilian tensile strength, Young's modulus, multiple regression, artificial neural network, Otanmäki, Finland

FOREWORD

Rock engineering and rock mechanics disciplines, relates to construction on and in rock masses of projects such as rock slopes, caverns, dams, hydroelectric schemes, mines and underground spaces for radioactive waste disposal. These subjects are evolving because of new capabilities provided by the utilization of computer programs which utilize knowledge of physico-mechanical properties of rocks in models to enhance quick inferences for critical decisions. Standard techniques for determining rock properties have been established over the years as guides for researchers. Estimates of these properties come in handy for engineers in determining the response of structures built in or on rocks for appropriate designs and remedies in mitigating failure scenarios.

The purpose of this work is to characterize selected physical and mechanical rock properties and compare multiple regression and ANN techniques in predicting models of uniaxial compressive strength, Young's modulus and Poisson's ratio. Due to strict technicalities involved in preparing core samples of regular geometry and the expensive nature of determining UCS (an essential parameter in most mining and rock engineering design), alongside Young's modulus and Poisson's ratio in similar testing procedure, simple models become attractive for inference purposes. Chapters 1 and 2 provides introduction and background to the topic. Chapter 3 details the methodology in carrying out the work from sampling, experimental tests, application of soft computing and the presentation of the test results. Discussions of the results are presented in chapter 4 and conclusions based on the discussions are outlined in Chapter 5. Finally, the summary of the work is illustrated in Chapter 6.

I am grateful to Renlund foundation for the award of grant in this study, Dr. Adeyemi Aladejare for his supervision of the work, Kimmo Kärenlampi for his suggestions and advice and Mr. Jouko Jylänki for his kind reception and grant of access to sites for the sampling. This is dedicated to my family and friends for their support in my life.

Oulu, 10.06.2020

Abubakar Osmanu

TABLE OF CONTENTS

LIST OF ABBREVIATIONS

A	surface area
ANN	artificial neural network
ASTM	American society for testing and materials
BTS	Brazilian tensile strength
C	load/area
C_0	compressive strength
D	diameter
d	diameter
d_0	initial diameter
E	elastic or Young's modulus
F	force
f	function
ISRM	International society for rock mechanics
kg	kilogram
LVDT	linear variable differential transducer
l	length
MLP	multi-layer perceptron
MSE	mean squared error
m_s	mass of solids or grains
m_{sat}	saturated mass
m_v	pore water mass

N	Newtons
n	porosity
n_0	initial porosity
P	peak load
RBF	radial basis function
RMSE	root mean squared error
SD	standard deviation
SSE	error sum of squares
SSR	regression sum of squares
SST	total sum of squares
T	temperature
T_0	tensile strength
t	thickness
UCS	unconfined compressed strength
VAF	variance accounted for
v	volume
ν	Poisson's ratio
var	variance
v_s	volume of solids
v_v	volume of voids
v_w	volume of water
w	water content
$\bar{Y}$	mean of measured values

$\hat{Y}_i$	predicted value for ith term
y	measured values
z	depth
Δd	change in diameter
Δl	change in length
ε	strain
εa	axial strain = change in length/initial length
εl	lateral strain = change in diameter/initial diameter
ρ	density = mass/volume
ρ_d	dry density
ρ_s	solid or grain density
ρ_{sat}	saturated density
σ	stress = load/area

1. INTRODUCTION

Rock has been utilized in construction since the dawn of civilization. Different structures have been built on, in or of rock, including houses, bridges, dams, tunnels, and caverns (Hoek, 2000; Zhang, 2004). In civil engineering, rocks are removed to make room for and /or incorporated in structures. In mining engineering, rocks are the material of interest being removed. The rock mass is the in-situ medium comprised of intact rock blocks separated by discontinuities such as joints, bedding planes, folds, sheared zones, and faults. Rock masses are discontinuous and often have heterogeneous and anisotropic properties. It is very difficult, therefore, to approach a rock engineering problem with confidence, especially in a non-precedent practice situation, without a coherent structured methodology (Hudson, 1993). It is in this light, that there is need to characterize rock technical properties to assist in predicting rock mass behavior when used in engineering structures.

Previous studies by (Aladejare, 2019) in evaluation of empirical estimation of uniaxial compressive strength of rock using measurements from index and physical tests indicates amongst others, the reliability of UCS estimated from empirical equations depends on the quality of the input data used in the equations. Also, fuzzy logic and ANN have been utilized for establishing predictive models in both mining and civil tunneling applications (Alvarez Grima and Babuska, 1999; Gokceoglu, 2002; Gokceoglu and Zorlu, 2004; Nefeslioglu et al., 2003, 2006; Sonmez et al., 2006; Kahraman et al., 2006; Yoo and Kim, 2007).

This study aims at characterizing physical and mechanical rock properties of two igneous rock types, gabbro and granite, from the Otanmäki area, central Finland. It seeks to establish correlation between different rock properties by developing and comparing predictive models using multiple linear regression and artificial neural network (ANN). Rock mechanical properties including uniaxial compressive strength (UCS), Brazilian tensile strength (BTS), Young's modulus, Poisson's ratio and rock physical properties such as density, porosity and water content were analyzed from 25 samples of the two igneous rock types.

2. THEORETICAL BACKGROUND

In recent times, radioactive waste disposal projects and the general use of underground space for hosting domestic refuse treatment, geothermal energy and large high-energy particle accelerators are being utilized in rock enclosed spaces. Table 2.1 lists different types of structures built on, in or of rock and the fields of their applications. Rock structures such as joints, bedding planes, folds, sheared zones, faults etc., render its form discontinuous and different from other engineering materials like concrete.

The rock mass is the in-situ medium comprised of intact rock blocks separated by discontinuities such as joints, bedding planes, folds, sheared zones, and faults. Intact rock in engineering terms is a rock containing no significant fractures (Zhang, 2017). The properties of the intact rock are governed by the physical characteristics of the materials of which it is composed and the way they are bonded to each other (Zhang, 2017). The properties used in description of intact rock include petrological name, colour, grain size, density, porosity, strength and hardness (Zhang, 2017). Rock masses are discontinuous and often have heterogeneous and anisotropic properties. An anisotropic rock has different properties in different directions (Harrison and Hudson, 1997).

Table 2.1 Application of different structures on, in or of rock (Zhang, 2017)

Field of Application	Types of Structures on, in or of Rock
Mining	Surface mining: slope stability; rock mass diggability; drilling and blasting; fragmentation Underground mining: shaft, pillar, draft, and stope design; drilling and blasting; fragmentation; cavability of rock and ore; amelioration of rockbursts; mechanized excavation; in situ recovery
Energy development	Underground power stations (hydroelectric and nuclear); underground storage of oil and gas; energy storage (pumped storage or compressed air storage); dam foundations; pressure tunnels; underground repositories for nuclear waste disposal;geothermal energy exploitation; petroleum development including drilling, hydraulic fracturing, wellbore stability

Transportation	Highway and railway slopes, tunnels, and bridge foundations;canals and waterways; urban rapid transport tunnels and stations;pipelines
Utilities	Dam foundations; stability of reservoir slopes; water supply tunnels; sanitation tunnels; industrial and municipal waste treatment plants; underground storages and sporting and cultural facilities; foundations of surface power stations
Building construction	Foundations; stability of deep open excavations; underground or earth-sheltered homes and offices
Military	Large underground chambers for civil defense and military installations; uses of nuclear explosives; deep basing of strategic missile

The subject of rock characterization is far more complex and intractable than might appear at first sight. The subject does not merely concern the optimal length-to-diameter ratio for a compression test specimen and other, similar tactical aspects of testing procedures: it concerns the whole strategic concept of how to characterize naturally occurring rock masses, which have been in existence for millions of years, have been operating as natural process - response systems for all that time and are about to be perturbed by engineers in order to achieve particular objectives (Hudson, 1992).

Rock mechanics is still based to a large extent on analytical techniques that were originally formulated for the mechanical design of structures made from man-made materials. The single most important distinction between man-made materials and the natural material rock is that rock contains fractures, of many kinds on many scales; and because the fractures – of whatever kind - represent breaks in the mechanical continuum; they are collectively termed "discontinuities". An understanding of the mechanical influence of these discontinuities is essential to all rock engineers. Most of the world is made of rock, and most of the rock near the surface is fractured. The fractures dominate the rock mass geometry, deformation modulus, strength, failure behaviour, permeability, and even the local magnitudes and directions of the in-situ stress field (Priest, 1993).

In a project, the stated objectives will require which rock properties will be required, the testing methods and how the site should be characterized (Hudson, 1993). Also, the material properties and the level of knowledge required, must vary with the project objective. This is the essence of rock characterization (Hudson, 1993).

2.1 ROCK CHARACTERIZATION

A consequence of the millions of years of mechanical, chemical and thermal processes to which the rock mass has been subjected is that it may well be anisotropic and inhomogeneous and associated with uncertainties (Aladejare and Wang, 2015, 2016a, 2017, 2019a, b; Harrison and Hudson, 1997; Phoon and Kulhawy, 1999). For this reason, rock mass characterizations of complex structures are crucial to recognizing their vulnerability as magnitude of knowledge-based uncertainties reduce as the level of knowledge increases (Baecher and Christian, 2003).

From a rock exposure, it is relatively easy to measure any property of the intact rock. Similarly, the rock mass structure is evident, and a good estimate of most discontinuity properties can be obtained. However, when it comes to large structures such as tunnels, obtaining information about rock mass properties is not an easy task. Because the amount of exposed rock is limited, testing has solely been on cylindrical lengths of borehole core. There are always constraints on resources, and so it is necessary when optimizing the rock characterization procedures to consider the requirements and to choose the rock access method and testing techniques in accordance with the engineering objective (Harrison and Hudson, 1997).

Two general categories for determining the engineering properties of rocks: direct and indirect method. The direct methods include laboratory and in situ tests whiles the indirect method includes empirical or theoretical correlation; a combination of intact rock and discontinuity properties; and back-analysis using field observation and prototype observation (Zhang, 2017). Generally, two direct methods of testing, known as destructive and non-destructive are used considering different aspects of structures (Barton, 2002). The non-destructive methods include ground penetrating radar (GPR) system, x-ray radiography and impact echo (IE) (Delatte et al., 2002; Locatelli et al., 2001). Although non-destructive methods are cost-effective and faster compared to destructive ones, they not often yield meaningful results because of not measuring the rock mass properties directly. The destructive methods can accurately determine the mechanical properties of rocks using direct mechanical tests in the laboratory. These methods are, however, time consuming and expensive (Zobach, 2007).

Since the early 1970s, the use of servo-controlled testing machines has provided an almost limitless capability for testing rock, the variation of which is only limited by the imagination (Hudson, 1993). Figure 2.1 (a) and (b) illustrate closed loop actions of testing machines (Hudson et al., 1972). Because the feedback control system can be arranged to control any variable, almost any test is possible. In the simpler cases, the stress rate or the strain rate can be controlled. Using the stress and strain together, the input energy can be controlled.

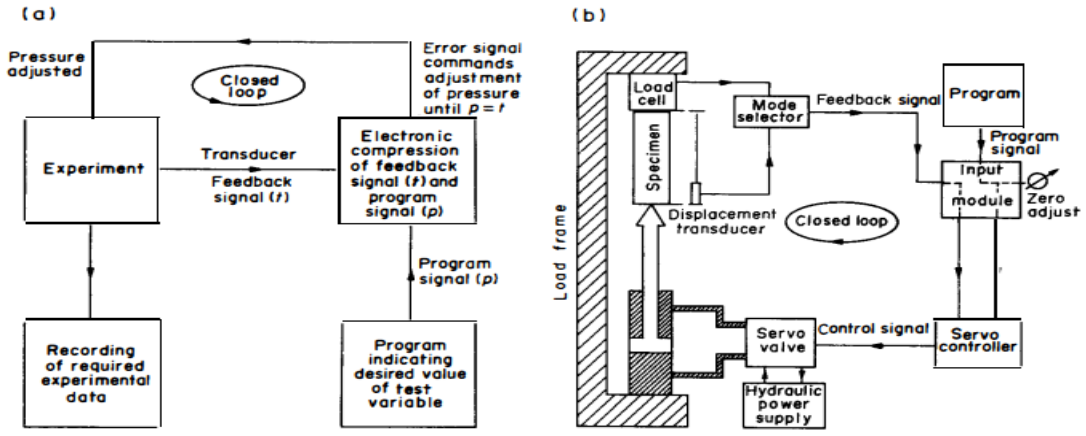

Figure 2.1 (a) The principle of closed-loop control and (b) Schematic of fast response, closed-loop, servo controlled testing machines (Hudson et al., 1972)

Standardized procedures are advantageous for measuring rock properties and site conditions. These standards among other advantages, provide; guidance which are helpful in conducting tests, the means of results comparison by different organizations on rocks at different sites, thereby enhancing knowledge sharing, a source of recommended procedures for use in contracts.

The International Society for Rock Mechanics Commission on Testing Methods (ISRM) has been producing Suggested Methods for rock testing and characterization since 1978, and these are widely used. There are also national bodies that produce standards for their own countries. In particular, the American Society for Testing and Materials (ASTM), via Committee D18.12, has produced an extensive series of methods for rock testing. There are many other countries which have their own wide range of standards (Harrison and Hudson, 1997). Table 2.2 lists some testing methods suggested by ISRM presented by (Ulusay,2014).

Table 2.2 List of all the ISRM Suggested Methods (SM) published between 1974 and 2014 (In chronological order) (Ulusay, 2014)

ISRM SUGGESTED METHODS
SM for Determining Shear Strength[a], [b]—1974
SM for Rockbolt Testing[a], [b]—1974
SM for Determining Water Content—Porosity—Density—Absorption and Related Properties and Swelling and Slake-Durability Index Properties[a], [b]—1977
SM for Monitoring Rock Movements Using Inclinometers and Tiltmeters[a], [b]—1977
SM for Determining Sound Velocity[a], [b]—1978
SM for Determining Tensile Strength of Rock Materials[a], [b]—1978
SM for Determining Hardness and Abrasiveness of Rocks[a], [b]—1978
SM for Determining the Strength of Rock Materials in Triaxial Compression[a], [b]—1978
SM for Monitoring Rock Movements Using Borehole Extensometers[a], [b]—1978
SM for Petrographic Description of Rocks[a], [b]—1978
SM for Quantitative Description of Discontinuities in Rock Masses[a], [b]—1978
SM for Determining in Situ Deformability of Rock[a], [b]—1979
SM for Determining the Uniaxial Compressive Strength and Deformability of Rock Materials[a], [b]—1979
SM for Pressure Monitoring Using Hydraulic Cells[a], [b]—1980
SM for Geophysical Logging of Boreholes[a], [b]—1981
SM for Determining the Strength of Rock Materials in Triaxial Compression: Revised Version[b]—1983
SM for Surface Monitoring of Movements across Discontinuities[b]—1984
SM for Determining Point Load Strength[b]—1985
SM for Rock Anchorage Testing[b]—1985
SM for Deformability Determination Using a Large Flat Jack Technique[b]—1986
SM for Deformability Determination Using a Flexible Dilatometer[b]—1987
SM for Rock Stress Determination[b]—1987
SM for Determining the Fracture Toughness of Rock[b]—1988
SM for Seismic Testing Within and Between Boreholes[b]—1988
SM for Laboratory Testing of Argillaceous Swelling Rocks[b]—1989
SM for Large Scale Sampling and Triaxial Testing of Jointed Rock[b]—1989
SM for Blast Vibration Monitoring[b]—1992
SM for Rapid Field Identification of Swelling and Slaking Rocks[b]—1994
SM for Determining Mode I Fracture Toughness Using Cracked Chevron Notched Brazilian Disc[b]—1995
SM for Deformability Determination Using a Stiff Dilatometerb—1996
SM for Determining the Indentation Hardness Index of Rock Materials[b]—1998
SM for Complete Stress-Strain Curve for Intact Rock in Uniaxial Compression[b]—1999
SM for in Situ Stress Measurement Using the Compact Conical-Ended Borehole Overcoring Technique[b]—1999

SM for Laboratory Testing of Swelling Rocks[b]—1999

SM for Determining Block Punch Strength Index[b]—2001

SM for Rock Stress Estimation—Part 1: Strategy for Rock Stress Estimation[b]—2003

SM for Rock Stress Estimation—Part 2: Overcoring Methods[b]—2003

SM for Rock Stress Estimation—Part 3: Hydraulic Fracturing (HF) and/or hydraulic testing of pre-existing fractures (HTPF)[b]—2003

SM for Rock Stress Estimation—Part 4: Quality Control of Rock Stress Estimation[b]—2003

SM for Land Geophysics in Rock Engineering[b]—2004

SM for Determining the Shore Hardness Value for Rock[b]—2006 (updated version)

SM for Determination of the Schmidt Hammer Rebound Hardness: Revised version[c]—2009

SMs for Determining the Dynamic Strength Parameters and Mode I Fracture Toughness of Rock Materials[c]—2012

SM for the Determination of Mode II Fracture Toughness[c]—2012

SM for Determining Shear Strength[a], [b]—1974

SM for Rock Stress Estimation—Part 5: Establishing a Model for the In situ Stress at a Given Site [c]—2012

SMs for Rock Failure Criteria (Six failure criteria)[c]—2012:

a. SM for Mohr-Coulomb Failure Criterion[c]

b. SM for the Hoek-Brown Failure Criterion[c]

c. SM for 3D Hoek-Brown Failure Criterion[c]

d. SM for Drucker-Prager Failure Criterion[c]

e. SM for Lade and Modified Lade 3D Rock Strength Criteria[c]

f. SM for a Failure Criterion for Rocks Based on True Triaxial Testing[c]

SM for for Measuring Rock Mass Displacement Using a Sliding Micrometer[c]—2013

SM for Rock Fractures Observations Using a Borehole Digital Optical Televiewer[c]—2013

SM for Determining the Mode-I Static Fracture Toughness Using Semi-Circular Bend Specimen[c]—2014

SM for Reporting Rock Laboratory Test Data in Electronic Format[c]—2014

SM for Determining Sound Velocity by Ultrasonic Pulse: Upgraded Version[c]—2014

SM for Determining the Creep Characteristics of Rock Materials[c]—2014

SM for Monitoring Rock Displacements Using Global Positioning System[c]—2014

SM for Laboratory Determination of the Shear Strength of Rock Joints: Revised Version[c]—2014

SM for Determining the Abrasivity of Rock by the Cerchar Abrasivity Test[c]—2014

SM for Step-Rate Injection Method for Fracture In-situ Properties (SIMFIP): Using a 3-Components Borehole Deformation[c]—2014

SM for the Needle Penetration Test[c]—2014

---

a Published in ISRM (1981, Yellow Book)

b Published in ISRM (2007, Blue Book)

c Published in ISRM (2014, Orange Book)

2.2 ROCK PROPERTIES

The intact rock material is separated into blocks by preexisting discontinuities. It may well be inhomogeneous, anisotropic, weathered which has overtime been subjected by a wide variety of natural mechanical, thermal and chemical processes. There may well be sets of discontinuities, each with a different genesis, resulting in a complex three-dimensional geometry with different discontinuities having different mechanical properties (Watkins et al., 2015; Zhang and Einstein; 2010, Najibi and Asef, 2014; Wyllie and Mah, 2004; Bery and Saad, 2012;).

It is usually helpful to have some understanding of the genesis of discontinuities, this may indicate something about either the discontinuity geometry or the mechanical properties, or both. The basic rock mechanics problem is the material rock to which either the applied stresses are changed or in which some new geometry is created (Hudson, 1995). Together, the intact rock and the discontinuities determine the rock mass properties. There is also a preexisting stress state. Then construction alters the stresses and changes the geometry (Hudson, 1995).

MECHANICAL PROPERTIES

Rock mechanical properties, such as strength (compressive, tensile and shear), Young's modulus, and Poisson's ratio, play an important role in wellbore stability, fracture prediction, and other engineering techniques (Chang et al., 2006; Abdulraheem et al., 2009).

Mechanical properties of rocks are usually measured using static and dynamic methods (Baoping and Hongzhi, 2005; Ai-Shayea, 2004). Static methods are generally conducted in the laboratory with specific test equipment that contain core specimens (Yuming and Guowei, 2000). The specimens are continuously compressed until failure occurs. Stress-strain curves are simultaneously recorded using a computer and mechanical parameters can be obtained from the curves.

Dynamic methods are usually calculations of compressional wave velocities (VP) and shear wave velocities (VS), which can be obtained from logs or in the laboratory (Guo

and Liu, 2014; Wen, 1998; Baoping and Economides, 2002; Ranjbar-Karami et al., 1998). Abundant studies regarding the differences between static and dynamic methods have demonstrated that static methods are more direct and realistic, while dynamic methods are easier and more continuous (Chang et al., 2006; Fjaer et al., 2008; Mavko et al., 2009). This study utilized static tests because of its capacity to control the rate of loading on test specimens, thereby providing valuable information of specimen response on the stress-strain curve.

In most cases, the rock mechanics information is obtained from tests on borehole core, so it is essential that the drilling report and borehole core logs are correctly completed and available (Hudson, 1993).In natural materials such as rock, it is important to know and understand its properties and behavior at the loading processes (Hudson and Harrison, 1997).

Analysis of mechanical properties are done using the stress-strain curve (figure 2.2). Stress is defined as the applied force per unit of area. Usually all failures can be qualified as certain stress quantities. Materials can be stressed at the same time by different types of stress. Stress is a tensor quantity, which means that it has magnitude, direction and "the plane under consideration" (Hudson and Harrison, 1997).

Under the influence of the forces, materials tend to deform. At compression, the axial length reduces while the diameter expands. When materials tend to elongate at tension, the diameter contracts. This phenomenon is called Poisson effect and termed, Poisson's ratio (Hudson and Harrison, 1997). Mathematically expressed as:

$$v = \frac{\varepsilon l}{\varepsilon a} \tag{1}$$

Where v is the poisson's ratio, εl is $lateral\ strain$, εa is $axial\ strain$

The axial strain is a ratio of change in length to initial length and it is expressed as:

$$\varepsilon a = \frac{\Delta l}{l} \tag{2}$$

Where εa is the axial strain, Δl is $change\ in\ measured\ axial\ length$ and l is the original measured length

The lateral strain is the ratio of the change in diameter to the original undeformed diameter. It can be expressed as:

$$\varepsilon l = \frac{\Delta d}{d_0} \tag{3}$$

Where εl is the lateral strain, Δd is change in diameter and d_0 is the original diameter.

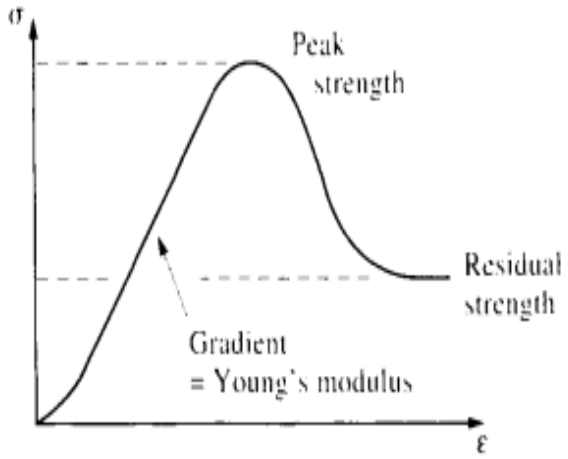

Figure 2.2 The complete stress-strain curve illustrating various mechanical parameters (Harrison and Hudson, 1997).

Researchers have investigated the effects of factors on the complete stress-strain curve and hence, mechanical properties of rocks (Funatsu et al., 2004; Rocchi et al.,2002; Sheinin et al.,2012; Nasseri et al.,2009; Liu et al.,2015; Jackson et al., 2008; Qi et al.,2009).

The elastic modulus increased with the ratio of specimen height to diameter and strain rate, whereas the Poisson's ratio was independent of these two factors (Liang et al., 2015). With regards loading conditions, (Jeong et al., 2007), stated that the compressive strength exhibited a positive correlation with strain rate, while the stress damage index hardly depended on strain rate. The physical and mechanical properties of limestone and granite under different temperatures by (Ozguven et al., 2014). They pointed out that the tensile strength of rocks decreased with increasing temperature, and the strength became much low for a temperature above 600°C. Understanding these variables, enhances the

prediction of mechanical behaviour of rock under conditions which may differ from those under which a specimen of the same rock was tested in the laboratory.

The process of rock failure is extremely complex and not subject to convenient characterization through simplified models. It may be either in terms of the precise details of each microcrack initiation and propagation, or in terms of the total structural breakdown as many microcracks propagate and coalesce (Harrison and Hudson, 1997). It is established that stress has been traditionally regarded as the ‘cause’ and strain as the 'effect' in materials testing. As consequence, early testing and standards utilized a constant stress rate application. Failure criteria have been developed to assist engineers in understanding failure properties and be able to predict when a rock is likely to fail.

This study investigates compressive strength, Brazilian tensile strength, Young’s modulus and Poisson’s ratio of the granite and gabbro cylindrical and discs specimens.

COMPRESSIVE STRENGTH

Compressive strength is the capacity of a material to withstand axially directed compressive forces. Rocks are seldom naturally loaded in one direction only, and most design procedures require some knowledge of the strength with stress applied in three principal directions. The most usual test for this condition, the triaxial cell system, has two of the principal stresses equal, and so lends itself to a two-dimensional analysis (Harrison and Hudson, 1997). That said, the most common measure of compressive strength is the uniaxial compressive strength or unconfined compressive strength (UCS). Usually compressive strength of rock is defined by the ultimate stress. It is one of the most important mechanical properties of rock material used in design, analysis and modelling.

In its simplest form, the uniaxial compression test is conducted by taking a right cylinder of intact rock, loading it along its axis and recording the displacement produced as the force is increased. In the curve shown in figure 2.4 as presented by (Harrison and Hudson,

1997), the various aspects of the mechanical behaviour of intact rock tested under these conditions can now be identified.

At the very beginning of loading, the curve has an initial portion which is concave upwards (the opposite of typical soil behaviour) for two reasons: (i) the lack of perfect specimen preparation, (ii) manifested by the ends of the cylinder being non-parallel; and (iii) the closing of microcracks within the intact rock.

After this initial zone, there is a portion of essentially linear behaviour, analogous to the ideal elastic rock. Another important parameter highlighted in Fig. 2.3 is the maximum stress that the specimen can sustain. Under the loading conditions shown in the diagram, the peak stress is the uniaxial compressive strength,σ_c.

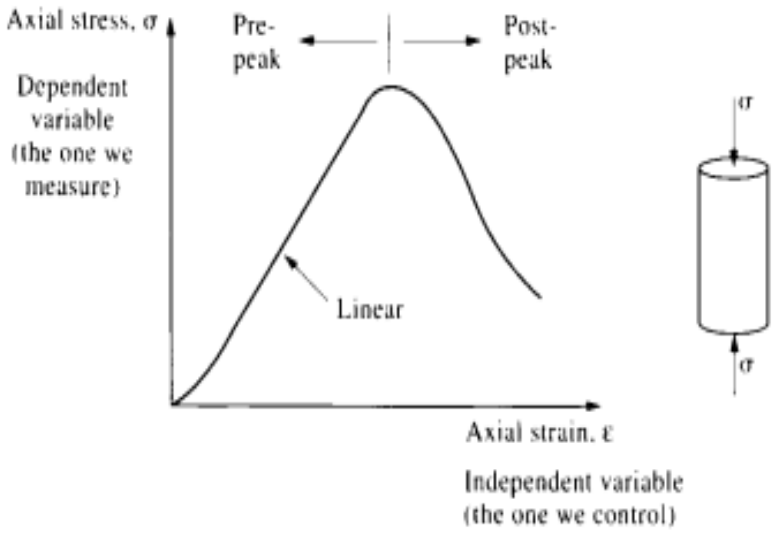

Figure 2.3. The complete stress –strain curve (Harrison and Hudson, 1997)

The specimen diameter in a UCS test is usually 1 in, but 2 in, 3/4 or 1/2 in sizes can also be used provided that the smallest dimension of the specimen is at least 10 times the maximum grain size. The length of the specimen, *l*, should be twice the diameter, d, but other lengths down to a 1: 1 ratio of *l*/d can be used, according to (Ulusay and Hudson. 2007).

For a specimen of diameter d and peak load P, the compressive strength is given as:

$$C_0 = \frac{P}{\pi d/4} \quad (4)$$

Where C_0 is the compressive strength in MPa, P in Nm^{-2} and d in m.

The ISRM suggested method (Ulusay and Hudson, 2007) specifies the test conditions much more closely, in that the diameter of the specimen should be not less than NX core 54 mm and the diameter(d), as the specimen specified as between d and d + 2 mm, with a thickness at least d/3 or 15 mm. The use of capping materials or end surface treatment other than machining to within 0.02 mm flatness is not permitted. Figure 2.4 illustrates the significant features, with the use of only one spherical seat being allowed (Hudson, 1995).

ISRM guidelines (Ulusay and Huudson, 2007) recommend that specimen ends be prepared to the following tolerances: ends perpendicular to the specimen axis within 0.001 rad; and ends flat to 0.02 mm.

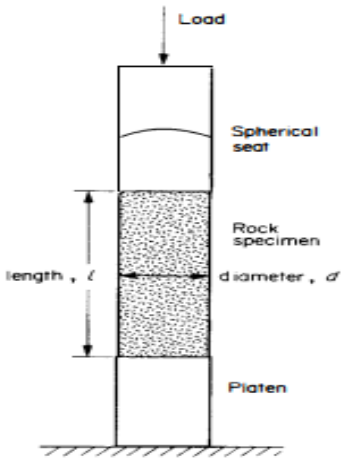

Figure 2.4. ISRM uniaxial compressive test (Hudson, 1995)

According to the ASTM D4543 (2008a) and ISRM suggested methods (Ulusay and Hudson, 2007), the lengths and diameter of the specimens are determined using an electronic caliper. The length is determined to the nearest 0.01 mm by taking an average of two lengths measured perpendicular to each other from the center of the end faces. The diameter is determined to the nearest 0.01 mm by taking the average of two diameters measured perpendicular to one another close to the top, middle, and bottom of the specimen.

TENSILE STRENGTH

Tensile strength of rock material is normally defined by the ultimate strength in tension, i.e., maximum tensile stress the rock material can withstand. Rock material generally has a low tensile strength. The low tensile strength is due to the existence of microcracks in the rock. The existence of microcracks may also be the cause of rock failing suddenly in tension with a small strain. Tensile strength of rock materials can be obtained from several types of tensile tests: direct tensile test, indirect tensile strength and Brazilian test. The most common tensile strength determination is by the Brazilian test.

The uniaxial tension test, as illustrated in Figure 2.5, is not as a rule used in engineering practice as direct test is not commonly performed due to the difficulty in sample preparation. Also, it is difficult to perform, and the rock does not fail in direct tension in situ (Harrison and Hudson, 1997).

Figure 2.5 Uniaxial tension (Harrison and Hudson, 1997)

The indirect tensile strength is the one measured when the tensile stress is generated by compressive loading. (The tensile strength of the rock is very much lower than the compressive strength, so that such indirect tests are possible, for the same reason, it is not possible to have indirect compression tests.). Through the testing configurations, the maximum tensile stress can be calculated from elasticity theory as a function of the compressive force and specimen dimensions. The tensile strength is, therefore, the maximum tensile stress calculated to be present in the specimen at failure (Harrison and Hudson, 1997).

Since the main problems in tensile testing of rock and similar materials are concerned with the very low strains which occur before failure, procedures generally attempt to apply

an even, direct stress by a loading system which avoids twisting or bending the specimen. The ISRM method (Ulusay and Hudson, 2007) specifies cores at least of NX size (54 mm), with the ends prepared smooth and flat as for the compressive strength test. Metal end caps of the same diameter are then cemented to the test specimen, and after hardening, the end caps are loaded by a chain linkage system. The number of tests possible depends on the specimens available, but at least five is preferred for calculating an average.

With the ASTM D3967 (2008b), the BTS specimens are drilled, cut, and then inspected to meet dimension tolerances including; smoothness of the cylindrical surface of the specimen shall be within 0.50 mm over the full length of the specimen; the perpendicularity of the specimen ends to the axis of the specimen shall not depart from a right angle by more than 0.5°. The BTS specimens are prepared with the thickness to diameter (t/D) ratio of 0.5.

In the Brazilian tensile stress test, according to elasticity theory, is developed across the vertical diameter of short cylinders diametrically line loaded. The specimen size is again specified as at least NX core, so that if cross drilling of cores is to be considered these must be at least HX size (approx. 70 mm).Spot loading of the short cylinders used (length of half diameter) must be avoided, and a layer of adhesive paper strip (masking tape) is wrapped round the specimen before loading in a slightly curved jig, as shown in figure 2.6. The tensile strength is calculated from the formula (Ulusay and Hudson, 2007):

$$T_0 = \frac{2P}{\pi D t} \tag{5}$$

Where T_0 is the tensile strength in MPa, P is the load at failure in kN, D is the diameter in mm and t, the thickness of the specimen also in units of mm.

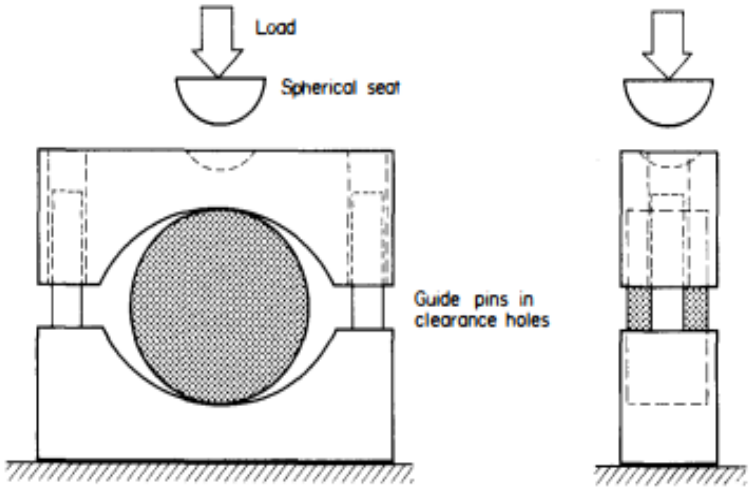

Figure 2.6. Apparatus for ISRM Brazil test (ISRM, 2007) from (Hudson, 1993)

YOUNG'S MODULUS

Young's modulus also known as the elastic modulus is an important parameter to describe stress and strain relationship. Young's modulus (E), is defined as the ratio of stress to strain, that is:

$$E = \frac{\sigma}{\varepsilon} \tag{6}$$

Where E is young's modulus in GPa, σ is stress in N/m^2, ε is strain

Elastic modulus describes the capacity of rock deformation, or the stiffness of a rock. For a high elastic modulus rock, it is less deformable (i.e. stiff). The initial part of the complete stress-strain curve will be steep. For a low elastic modulus (soft) rock, it is more deformable, and the initial part of the complete stress-strain curve will be gentle (Hudson and Harrison 1997).

It can be determined in two ways: either by taking the slope of the stress-strain curve at a given point; or by taking the slope of a line connecting two points on this linear portion of the curve (Fig. 2.7). The two slopes are the tangent modulus and the secant modulus. The tangent modulus is conventionally taken as the gradient of the $\sigma - \varepsilon$ curve at a stress level corresponding to 50% of the peak stress; the secant modulus may be determined

anywhere over the entire linear portion. Naturally, both of these are approximations to the real behaviour, but are useful and adequate for simple elastic applications.

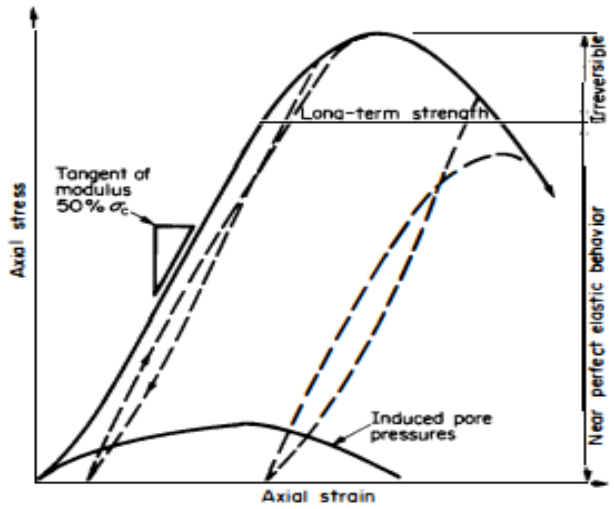

Figure 2.7. Typical stress-strain curve showing tangent modulus computation (Hudson, 1995).

Young's modulus (E50) is calculated for every Uniaxial Compressive Strength (UCS) test using the ASTM D7012 (2014) standard. Young's modulus, E, is defined as the average slope of the straight-line portion of the stress-strain curve, calculated between 40 and 60 percent of the maximum applied load as:

$$E = \frac{change\ in\ axial\ stress}{change\ in\ axial\ strain}\ \ over\ interval\ of\ 30-50\%\ of\ UCS \tag{7}$$

Where E50 represent the standard values normally reported, this range of behaviour overlaps with the onset of damage initiation and is therefore subject to inelastic influences.

POISSON'S RATIO

Poisson's ratio is the ratio of transverse strain to corresponding axial strain on a material stressed along one axis, at linearly elastic region. For a rock core subjected to axial load, Poisson's ratio (v) can be expressed mathematically as indicated in equation (1).

For design problems it is important to assess the in-situ deformation parameters of a rockmass (Hudson, 1995). A step in this process is measurement of the axial and lateral

strain response in uniaxial compression. Although the terms Young's modulus and Poisson's ratio are strictly only true for a linearly elastic material, they are used for the deformation characteristics of rock either as tangent or secant modulus values.

Measurement of axial and lateral stress-strain curves is best done using resistance wire strain gauges cemented to the test specimen (Komurlu, 2018). These devices usually involve displacement transducers such as linear variable differential transformers (LVDTs).

Poisson's ratio (v50) is calculated for every Uniaxial Compressive Strength (UCS) test using the ASTM D7012 (2014) standard according to:

$$v = \frac{change\ in\ axial\ stress}{change\ in\ axial\ strain}\ \ over\ interval\ 30 - 50\%\ of\ UCS \tag{8}$$

Where v50 represent the standard values normally reported, this range of behaviour overlaps with the onset of damage initiation and is therefore subject to inelastic influences.

For most rocks, the Poisson's ratio is between 0.15 and 0.40 (Figure 2.8). At a later stage of loading beyond linearly elastic region, lateral strain increases faster than the axial strain and hence lead to a higher ratio.

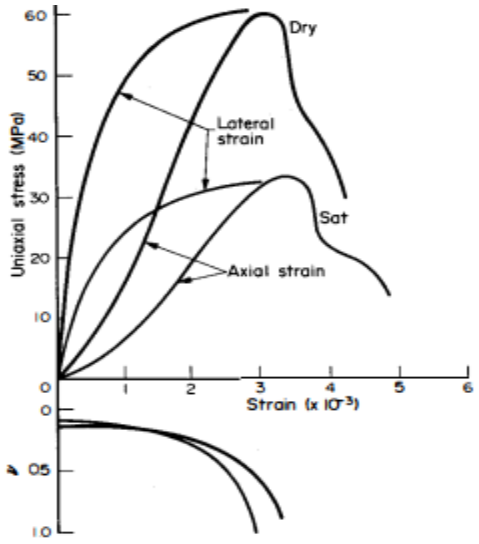

Figure 2.8. Typical stress-strain curves in uniaxial compression tests (Hudson, 1995)

2.2.3 PHYSICAL PROPERTIES

Physical properties of a rock relevant to geomechanics applications include its mass density, porosity, water content. The techniques that can be used to measure these properties range from weighing, drying and measuring the volume of the specimen as suggested by ISRM (Ulusay and Hudson, 2007) to more complicated experiments such as mercury intrusion porosimetry (Léon Y León, 1998) or x-ray diffraction and fluorescence. These tests are important for the proper characterization of the rock as well as for development and implementation of computational models that can be used in prediction exercises (Selvadurai and Nguyen, 1995; Alonso et al. 2005). This study deals with the density, water content and porosity of gabbro and granite samples. The chemical composition tests were performed using x-ray techniques.

DENSITY

Density is defined the mass per unit volume of a material. Since a rock contains both grains (solid matrix material) and voids, it is necessary to distinguish between different densities which are related to different parts or components of the rock, as defined in Table 2.4 (Zhang, 2017). It is usually expressed in g/cm^3. The density of rocks depends on the mineral composition, the porosity and the filling material in the voids (Zhang, 2017).

Table 2.4 Definitions of various density terms (Zhang, 2017)

Term and definition	Equation
Density (or bulk density): Mass determined at natural water content	$\rho = \frac{m}{v}$
Dry density: Mass refers to solids only. All moistures dried out of the voids	$\rho_d = \frac{m_s}{v}$
Saturated density: Mass refers to solids and water which fills the voids	$\rho_{sat} = \frac{m_{sat}}{v}$

Grain density (or solid density): Both mass and volume refer to the grains (solids) only $\rho_s = \frac{m_s}{V_s}$

where m = m_s+ m_w and V = Vs + Vv in which m is the bulk sample mass, m_s is the mass of the grains(solids), m_w is the mass of water in the voids, V is the bulk sample volume, Vs is the volume of the grains (solids), and Vv is the volume of the voids.

The density of rocks can be determined using the method suggested by ISRM (2007). The parameters for the calculation of density after following the suggested procedures are determined from the equations as follows:

$$Saturated - surface - drymass\ (M_{sat}) = B - A \quad (9)$$

$$Grain\ weight\ (M_s) = C - A \quad \text{(kg)} \quad (10)$$

$$Bulk\ volume(V) = \frac{M_{sat} - M_{sab}}{\rho_w} \quad (m^3) \quad (11)$$

$$pore\ volume(V_v) = \frac{M_{sat} - M_s}{\rho_w} \quad (m^3) \quad (12)$$

$$Porosity\ (n) = \frac{100V_v}{V}\ \% \quad (13)$$

$$Dry\ density\ of\ rock\ (\rho_d) = \frac{M_s}{V} \quad \left(\frac{kg}{m^3}\right) \quad (14)$$

Where A is mass of sample container in (kg), B is the mass of sample container and saturated dry mass of sample in (kg) and C is the mass of the container plus oven dry mass of sample, also in units of (kg).

Density and porosity often related to the strength of rock material. A low density and high porosity rock usually has low strength.Rock density is controlled by densities and volumetric fractions of components which the rock is composed. Therefore, density differences between minerals, fluids, and gases cause a strong correlation between rock density and porosity. For underground rocks, as depth increases the rock compaction increases, causing porosity reduction (Peng and Zhang, 2007).

POROSITY

The (total) porosity, n, is defined as the ratio of void or pore volume (Vv), to the total volume (V), of the rock:

$$n = \frac{V_v}{V} = \frac{V - V_s}{V} \tag{15}$$

Where Vs is the volume of the grains or solid matrix substance. Porosity is usually given as a percentage. The porosity of rocks can be determined by using the method suggested by ISRM (2007) and utilizing equation (13).

Porosity is the result of various geological, physical, and chemical processes and varies significantly for different rock types. Porosity changes significantly even for the same rock type due to different factors such as grain size distribution, grain shape, depth/pressure, and temperature. Figure. 2.9 shows the variation of porosity n with mean grain diameter d_{50} for Bentheim Sandstone (Schön, 1996) as reported by (Zhang, 2017).

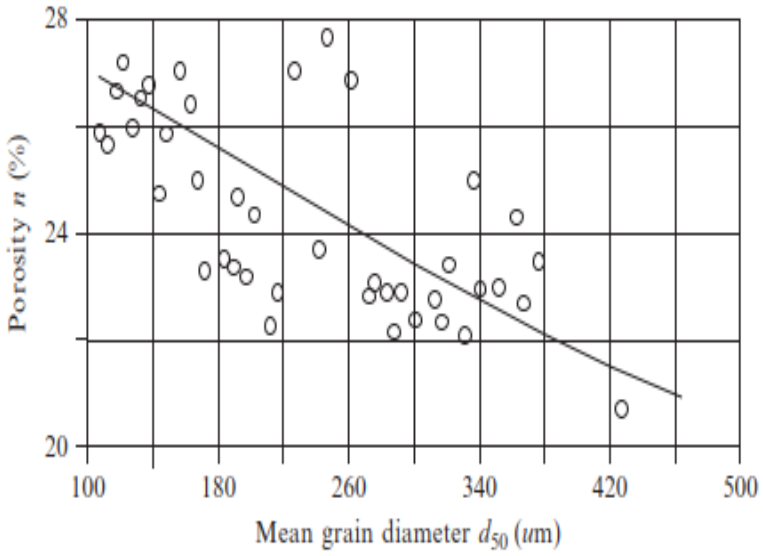

Figure 2.19. Porosity n versus mean grain diameter $d_{50\ (\mu m)}$ for Bentheim Sandstone. (Zhang, 2017).

Porosity is primarily controlled by the shape, size and arrangement of the rock grains (Peng and Meng 2002). It also depends on rock mechanical processes (such as compaction, deformation, fracture evaluation etc.) and geochemical processes (e.g. dissolution, precipitation, mineralogical changes).

WATER CONTENT

Water content is a measure indicating the amount of water the rock material contains. It is simply the ratio of pore water volume to the bulk volume of the rock material. It can be expressed as:

$$w = \frac{V_w}{V_s}\ x\ 100 \tag{16}$$

Where w is the water content in (%), v_w is the pore water volume and V_s is the volume of rock.

The water content of rocks can be determined using the method suggested by ISRM (2007). The parameters for the calculation of water content after following the suggested procedures are determined from the equations as follows:

$$water\ content\ w = \frac{pore\ water\ mass(M_v)}{grain\ mass\ (M_s)}\ x\ 100\% \tag{17}$$

$$= \frac{B - C}{C - A}\ x\ 100\%$$

Where A is mass of sample container in (kg), B is the mass of sample container and saturated dry mass of sample in (kg) and C is the mass of the container plus oven dry mass of sample, also in units of (kg).

According to ASTM D2216 (2010), the water content by mass of each specimen is calculated once the final dried mass has been measured and it is recorded to the nearest 1% and is calculated using Equation:

$$w = \left(\frac{M_{cms} - M_{cds}}{M_{cds} - M_c}\right)\ x\ 100 \tag{18}$$

Where w is water content (%), M_{cms} is the mass of the container and moist specimen (g), M_{cds} is the mass of the container and oven-dried specimen (g), and M_c is the mass of the container (g).

According to (Zhang, 2017), water content has a great effect on the deformability of intact rock. The elastic modulus of intact rock decreases as the water content increases. For example, the experimental data of the massive gypsum of the Hafik formation in the Sivas basin (Fig. 2.10) show that the elastic modulus decreases with the water content approximately following the relation below (Yilmaz, 2010):

$$E = 13.23e^{-0.4701w} + 9.3 \ (r^2 = 0.92) \quad (19)$$

Where E is the elastic modulus in GPa; w is the water content in %; and r^2 is the determination coefficient.

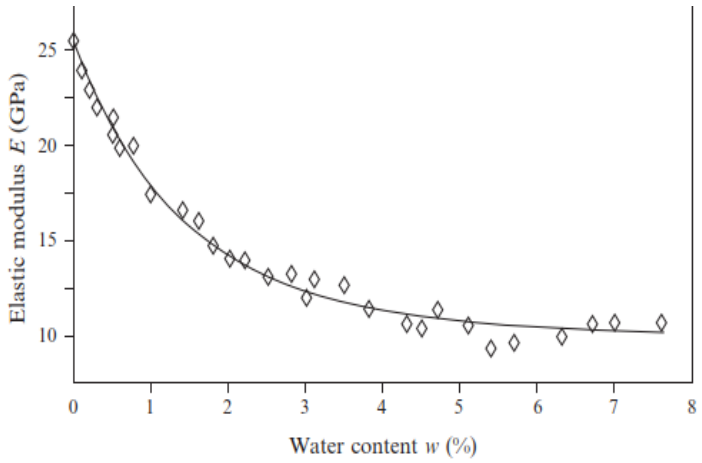

Figure 2.10. Influence of water content (w) on elastic modulus E for gypsum. (Yilmaz, 2010)

2.3 PETROGRAPHY AND THIN SECTION PREPARATION

The petrographic observations under microscope display not only the textures of rocks but also reveal the order of formation of minerals and provide some important clues about the mechanism of petrogenesis as well. They also influence the mechanical behaviour of rocks to a certain degree (Hu et al., 2014). According to (Hu et al., 2014), strength tended to improve as the ratio between soft to hard minerals, ratio between secondary to primary phases and the degree of serpentinization decreased. The alteration features, including mineralogical reform, disruption of existing textures and initiation of new cracks caused a reduction of strength of granites (Basu et al., 2009).The effect of

weathering/ alteration on porosity and compressive strength of various rock types from Turkey was presented by (Tugrul, 2004).

The modal mineralogical composition and microfabric characteristics of rocks are described in (Prikryl, 2006; Prikryl et al., 2007).The textural features cast much light on the conditions under which an igneous rock consolidates from its present magma, for it is controlled by the rate and order of crystallization, and these in turn depend on the initial temperature, composition, content of fugitive components, viscosity of the magma and the pressure under which it solidifies. Detailed petrographic work is a necessary step in classification, an aid to on-going field investigations, a prerequisite to geochemical and geochronological work, and an essential component in making petrogenetic inferences (ISRM 2007).

The micro-petrographic description of rocks for engineering purposes includes the determination of all parameters which cannot be obtained from a macroscopic examination of a rock sample, such as mineral content, grain size and texture, and which have a bearing on the mechanical behaviour of the rock or rock mass. A common form of microscopic examination employed for transparent materials involves the use of thin sections and refracted light. Opaque materials can be sawed and polished and then examined using reflected light techniques (ISRM, 2007).

The (ISRM, 2007) stipulates that, to ensure its correct classification, the first step should be to ascertain the mineral composition and texture of the rock. Further investigations should include a fabric and mineral analysis in the case of strongly anisotropic rocks, the determination of the degree of alteration or weathering, grain size, micro-fracturing and porosity.

In thin section preparation, the ISRM 2007 suggested method requires that in order to obtain a representative sample of the rock, more than one specimen should be selected during field work. Wherever possible, oriented specimens should be collected and the original strike and dip of one face of the specimen should be recorded.

2.4 REGRESSION ANALYSIS

Regression analysis or curve fitting consists arriving at a relationship that may exist between two or more variables. In the context of experiments, the variables represent

cause(s) effect relationship, with a measured quantity depending on other measured quantities (Venkateshan, 2015). Regression analysis is a way of fitting a “best” line through a series of observations. With “best” line we mean that it is fitted in such a way that it minimizes the sum of squared differences between the observations and the line itself (Mooi, 2014).

In statistics, regression analysis includes many techniques for modeling and analyzing several variables, when the focus is on the relationship between a dependent variable and one or more independent variables. More specifically, regression analysis helps one understand how the typical value of the dependent variable changes when any one of the independent variables is varied, while the other independent variables are held fixed (Manouchehrian et al., 2013). In all cases, the estimation target is a function of the independent variables called the regression function. A regression model relates Y to a function of X and b as below:

$$Y \approx f(X, \beta) \tag{20}$$

Where Y represents the dependent variables, X the independent variables and β the unknown parameter, which may be a scalar or a vector.

A regression model can be in linear or non-linear form. In linear form, the parameters of the model are assumed to be linear but in non-linear form, these parameters are non-linear. Due to simpler computations and statistical analyses of linear regression models, these kinds of models are more common to use for regression analysis. General form of a linear regression model for modeling n data points and p independent variables is:

$$y_i = \beta_0 + \beta_1(x_{1i}) + \beta_2 f_2(x_{2i}) + \beta_3(x_{3i}) + \ldots + \beta_p(x_{pi}) + \varepsilon_i \tag{21}$$

where β_0 is the intercept, $\beta_{1\ldots}\ \beta_p$ are the slope between Y and the appropriate $x_{i,}$ ε_i is the error term that captures errors in measurement of Y and the effect of Y on any variables missing from the equation that would contribute to explaining variations in Y.

Nonlinear regression methods are in the form power, exponential, logarithmic (Yagi et al., 2009; Hoek et al., 2002; Langford and Diederichs, 2015), and only recently Bayesian

regression models have become available (Bozorgzadeh et al., 2018a, b; Contreras et al., 2018).

The simple regression analyses provide a means of summarizing the relationship between two variables (Yagiz et al., 2009). The limitations however are that, most relationships are not linear, and models developed therefrom, become statistically insignificant.

Multiple regression generally, is to learn more about the relationship between several predictor variables and a dependent or criterion variable. The performance of the model depends on many factors that act and interact in a complex manner (Kumar et al., 2013). It is widely used for modelling and analyzing the experimental results.

The least square error method is a very common method to evaluate the unknown parameters for a given data set. A large body of techniques for carrying out regression analysis has been developed. Familiar methods such as linear regression and linear least squares regression are techniques, in which the regression function is defined in terms of a finite number of unknown parameters that are estimated from the data. In linear least square method, the unknown parameters are evaluated somehow to minimize the sum of squared error in which the error is the difference between observed and evaluated values of the dependent variable. For a linear regression, the sum of squared error defines as:

$$SSE = \sum(Y_i - \hat{Y}_i)^2 \tag{22}$$

$$SSR = \sum(\hat{Y}_i - \bar{Y})^2 \tag{23}$$

$$SST = (Y_i - \bar{Y})^2 \tag{24}$$

$$SST = SSR + SSE \tag{25}$$

$$R^2 = 1 - \frac{SSE}{SST} = \frac{SSR}{SST} \tag{26}$$

Where SSE (error sum of squares) is the sum of squared deviations of observed values from predicted values, SSR (regression sum of squares) is the sum of squared deviations of predicted values from the mean, SST (total sum of squares) is the sum of total

deviations about the mean, Y_i is the observed value for i, $\hat{Y}_i$ is the predicted value for i, $\bar{Y}$ is the mean for the observed values.

The performance of regression analysis methods in practice depends on the form of the data generating process, and how it relates to the regression approach being used

Regression analysis within recent years has seen a steady increase and successful application in many areas of rock mechanics and engineering. For example, (Kahraman, 1999) developed some regression models to predict penetration rates of rotary and percussive drills. (Bozorgzadeh et al., 2018a) discussed how to formulate frequentist and Bayesian regression models for analysis of intact rock strength data. This work pays attention to the form and location of variability in rock strength data. (Tugrul and Zarif, 1999) described the relationships between mineralogical and textural characteristics with engineering properties of some selected granite rocks by simple regression analyses. (Katz et al., 2000) established empirical correlation between rebound readings of Schmidt Hammer and laboratory measured values of Young's modulus, uniaxial strength and dry density.

(Karakus et al., 2005) used multiple regression modelling technique to predict elastic properties of intact rocks from index tests. Research to investigate the effect that different combinations of compressive and tensile strength results have on the values of uncertainties in m, compressive strength and standard deviation of axial strength. Two secondary investigations have been performed, one examining the ratio between direct and indirect tensile strengths, and the other examining the evidence for a tensile cut-off in the H-B criterion. The subject of the analysis is an extensive strength dataset of medium-grained metagranite granodiorite occurring at the Swedish Nuclear Fuel and Waste Management Company (SKB) Forsmark site, Sweden (Elorant, 2004a, b, c; Jacobsson, 2004a, b, c, 2006, 2007; Gorski and Conlon, 2007).

The key benefits of using regression analysis are that it can; indicate significant relationship or otherwise of it between dependent and independent variables, indicate the

relative strength of different independent variables' effects on a dependent variable, and make predictions.

2.5 ARTIFICIAL NEURAL NETWORK (ANN)

Artificial Neural Networks (ANN) is one of soft computing techniques whose guiding principles is to exploit the tolerance for imprecision, uncertainty, and partial truth to achieve tractability, robustness, low solution cost, better rapport with reality (Ibrahim, 2016). It is one the initial learning machines developed in the 1940s based on the biological neuron system of human brains. It found its application later in the 1980s and has been used for many engineering related applications ever since, due mainly to its capability in extracting complex and non-linear relationships between features of different systems (Artun et al., 2005; Gholami et al., 2014;Abbaszadeh et al., 2016).

In neural computation, the artificial neurons are designed as variations on the abstractions of brain theory and implemented in software or other media and it is the biological neurons that inspired the various notions of formal *neuron* used in neural computation (Negnevitsky, 2002;Arbib, 1995).When a neuron receives excitatory input that is sufficiently large compared with its inhibitory input, it sends a spike of electrical activity down its axon (Park, 2011). Learning occurs by repeated adjustments of numerical weights assigned to the neurons (Park, 2011; Negnevitsky, 2002).

The performance and computational complexity of NNs are mainly based on network architecture, which generally depends on the determination of input, output and hidden layers and number of neurons in each layer. The number of layers and neurons in each layer affect the complexity of NN architecture. NN architectures are discussed at length in several research works (Öztütk, 2003). A single hidden layer is sufficient for the ANN to approximate any function and to any arbitrary given accuracy. Use of more than a single layer can lead to many local minima and make the training difficult (Hornik et al., 1989).

In the literature, there are several networks such as Hopfield networks, adaptive resonance theory networks, Kohonen networks, backpropagation networks, recurrent networks, counter propagation networks, multi-layer perceptron networks, radial basis function networks, etc. Multi-layer perceptron (MLP) and radial basis function (RBF) are two of the most widely used neural network architecture. They are robust predictors with the ability to generalize for imprecise input data. General difference between MLP and RBF is that RBF is a localized type of learning which is responsive only to a limited section of input space. On the other hand, MLP is a more distributed approach (Kumar, 2013). In MLP for instance, the weighted sum of the inputs and bias term are passed to activation level through a transfer function to produce the output and the units are arranged in a layered feed-forward topology called Feed Forward Neural Net- work.

Various activation functions perform a mathematical operation on inputs to a specified output. The function could be linear and be expressed mathematically as:

$$Y = f(u) = \alpha.u \tag{27}$$

Where α is the slope of the linear function, Y, the output and u, input function.
The activation function may be non-linear sigmoidal (S shape) and expressed as:

$$f(x) = \frac{1}{1 + e^{-\alpha x}} \ , 0 \leq f(x) \leq 1 \tag{28}$$

Where α is the shape parameter of the sigmoid function.

The tangent sigmoidal function is another non-linear activation function used and mathematically expressed as:

$$f(x) = \frac{2}{1+ e^{-\alpha x}} - 1, \ -1 \leq f(x) \leq +1 \tag{29}$$

As each input is applied to the network the network output is compared with the actual target value and the error is calculated. The error between the network output and the actual output is minimized by modifying the network weights and biases (Park, 2011;

Negnevitsky, 2002). The goal is to minimize the average of the squares of the errors which is called Mean Square Error of the output.

$$Mean\ squared\ error\ (MSE) = \frac{1}{Q\ \sum_{k=1}^{Q}(t(k)-a(k))^2} \quad (30)$$

Where t(k) is the actual value, a(k) is the network value and Q is the number of epochs. When the MSE falls below a predetermined value or the maximum number of epochs have been reached, the training process stops.

A trained neural network can be used for simulating the system outputs for the inputs which have not been introduced before. The coefficient of determination (R^2) between the actual and predicted values is a good indicator to check the prediction performance of each model. Furthermore, in this study, variance account for (VAF) and root mean square error (RMSE) indices were calculated to control the prediction performance of the model. When R^2 is 1, VAF is 100 and RMSE is 0, then the model is excellent. R^2 is expressed mathematically as represented in equation (35). VAF and RMSE as expressed as below:

$$VAF = \left[1 - \frac{var(y-y')}{var(y)}\right] X\ 100 \quad (31)$$

$$RMSE = \sqrt{\frac{1}{N}\sum_{i=1}^{N}(y-y')^2} \quad (32)$$

Where y and y′ are the measured and predicted values respectively.
According to (Haykin,1999), all data should be divided into two data sets such as: training (70% of all data) and test (30% of all data).

During training in ANN technique, overfitting, which occurs when huge number of data and a very complicated function is selected to reduce the empirical risk. huge number of data and a very complicated function is selected to reduce the empirical risk. This leads to a very promising result often yielded at the training stage, but a poor estimation is achieved at the testing step by the machine (Martinez-Ramon and Cristodoulou, 2006; Duda et al., 2002). This is often resolved by reducing the complexity of the model used to explain the data (Abe, 2008).

ANN have been used to develop multiple prediction models for prediction of rock parameters in engineering geology (Sonmez et al., 2006; Singh et al., 2007; Haykin, 1999; Gokceoglu and Zorlu, 2004; Ceryan et al., 2012; Yesiloglu-Gultekin et al., 2013). These studies have indicated that ANNs are effective approaches when compared with analytical predictive models Methodologies for estimating various geotechnical properties of rocks including permeability, compression index, shear strength etc., have been successfully developed with the application of ANN (Ozer et al., 2008; Park et al., 2009; Park and Kim, 2010; Park and Lee, 2010; Najjar and Ali, 1999; Penumadu and Zhao, 1999).

The behavior of pile foundations erected in soils is considerably uncertain, sophisticated with less understanding (Baik, 2002). For this reason, ANN has also been applied in the bearing capacity of pile (Bea et al., 1999; Goh et al., 2005; Abu-Kiefa, 1998; Das and Basudhar, 2006, Park and Cho, 2010) in areas such as the modeling the axial and lateral load capacities of deep foundations. It has also been utilized in the design and construction of tunnels and underground openings (Shi, 2000; Yoo and Kim, 2007) as well as in slope stability analysis (Neaupane and Achet, 2004; Ferentinou and Sakellariou, 2007; Zhao, 2007; Cho, 2009)

ANNs have many advantages such as fast prediction responses, noise suppression capabilities, ability to handle large amount of data, and the ability to model complex relationships between the inputs and the outputs without the need for having knowledge about the underlying distributions in the data (Haykin, 1999).

3. METHODOLOGY

The experimental tests in this study was to examine the influences of various test parameters on the geomechanical properties of two igneous rocks, gabbro and granite from Otanmäki area, central Finland. The conduct of UCS test in association with deriving Young's modulus and Poisson's ratio of a specimen is quite expensive and comes with strict specimen preparation standards. This study sought to compare the predictive capacities of regression and ANN models to estimate UCS, Young's modulus and Poisson's ratio using experimental data from their corresponding BTS, density, porosity and water content.

In this section, the methodology used to collect, prepare and test Uniaxial Compressive Strength (UCS), Young's modulus, Poisson's ratio and Brazilian Tensile Strength (BTS) of the specimens will be discussed. This entails the retrieval of samples, the drilling, cutting and grinding of specimens, specimen testing condition preparation, the procedures and equipment used during testing and calculations used to estimate the properties. In addition, test methodology and modes used to calculate properties such as water content, porosity and bulk density will also be explained. Multiple linear regression and Artificial neural network (ANN) techniques used to construct models of the rock properties are mentioned. The results of testing will be presented and discussed with respect to specimen condition and ability to accurately characterize the geomechanical properties of the two rocks.

3.1 SITE VISIT AND SAMPLE PREPARATION

Sampling locations within the Otanmäki area, central Finland, close to the Otanmäki Fe-Ti-V deposit was selected for this work. The Otanmäki area is located 150 km southeast of Oulu in Vuolijoki, within the bounds of the Kajaani municipality in Central Finland. To the southwest of Otanmäki is lake Saaresjärvi, and Oulujärvi lake to the north (Figure 3.1 A).

Two sampling sites at Vuorokas for the gabbro and Pikkukallio for the granite were made available by Jouko Jylänki, the CEO of the Otanmäki Mine (Fig. 3.1B).Large boulders (0.5 x 0.3 x 0.3 m) of each rock type were taken for further processing at the Oulu Mining School (OMS).

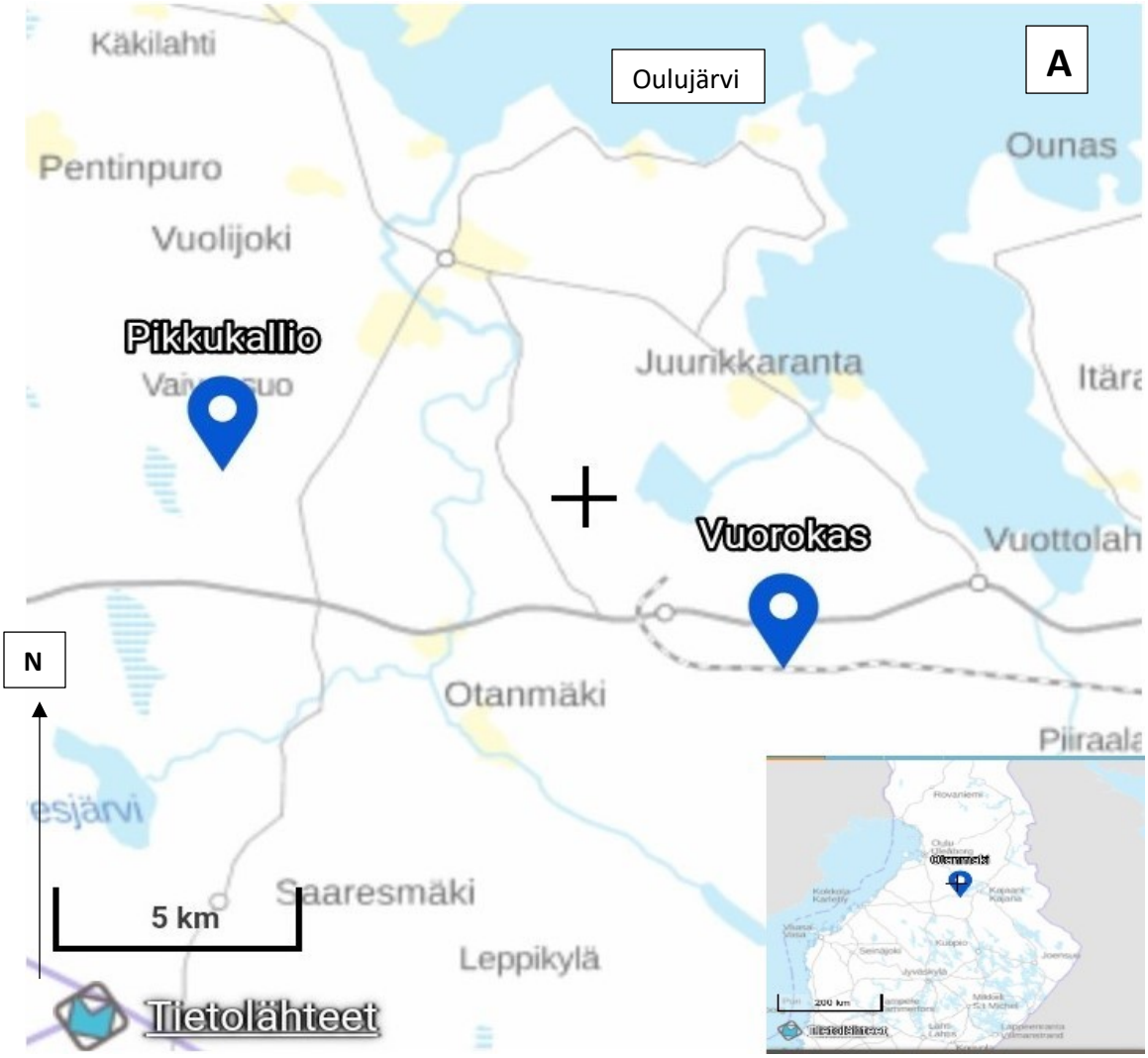

Figure 3.1. (A) Map of Finland showing Otanmäki area in central Finland with approximate locations of the sampling sites at Pikkukallio and Vuorokas (Maanmittauslaitos, 2020) (B) sampling site at Vuorokas (photograph by Kimmo Kärenlampi).

The UCS specimens were prepared in accordance with the ISRM suggested method (Ulusay and Hudson, 2007). Cylindrical specimens were retrieved by coring from the boulders with a Hilti DD 110-W diamond handheld core drilling machine (Fig. 3.2). The specimens for the UCS and BTS tests were cut and preliminary grinding of the surfaces done at the Oulu mining school (OMS) with a diamond saw. These specimens are labelled (SA01-15) for the gabbro and (SB01-10) for the granite (Fig.3.3).

The UCS specimens were cut to the final length of the specimen with an additional length of 2 to 3 mm for grinding. If the length of the cores permits, BTS specimens were also cut from the top and bottom of the UCS specimens. While cutting the BTS specimens, special care was taken to ensure that the ends remain parallel to one another in accordance with ISRM testing standards. Fifteen (15) cylindrical and disc shaped samples were investigated for the UCS and BTS respectively, of the gabbro and ten (10) cylindrical and disc shaped specimens were investigated for the UCS and BTS of granite. The UCS specimens used in this testing had a mean diameter of 54.6 mm and a consistent length to

diameter ratio (L/D) of 2.0. The BTS specimens had an average diameter of 54.6 mm and a consistent thickness to diameter ratio (t/D) of 0.5.

The final grinding to within testing standards was done at the Aalto university school of engineering with a Form+Test PSM 3/230 specimen grinder meeting the ISRM, 2007 standards. Figure 3.4 shows some of the specimens after regrinding. Fourteen of the twenty-five cylindrical specimens, however, were not in the best of shapes for testing standards, these specimens were either having ends not perpendicular to the axis or were not having uniform circumference (Fig. 3.5). UCS tests were conducted, regardless, to observe variations in the results.

The accuracy of the length and diameter measurements meets the requirements of ASMT D4543 (2008a) and ISRM suggested methods (Ulusay and Hudson, 2007).The nominal diameter of the specimens were 54mm and their length to diameter (L/D) ratio was 2:1 with regards the UCS test specimens as recommended by ISRM, (Ulusay and Hudson, 2007). The BTS test specimens had also, a nominal diameters of 54.6 mm and thickness ranging from (2.6-2.9mm) with a thickness to diameter ratio (t/D) of approximately 0.5, satisfying the testing standards for the ISRM (International Society for Rock Mechanics) (Ulusay and Hudson 2007) and ASTM D3967 (2008b).

Samples of the same rock type for both gabbro and granite were crushed to about 10-12mm size for the conduct of the density, porosity and water content determination. Also, thin section blocks were cut for preparation of polished thin sections.

Figure 3.2. Drilling core samples from the boulders drilling at the Oulu Mining School (OMS) (photographs by Kimmo Kärenlampi)

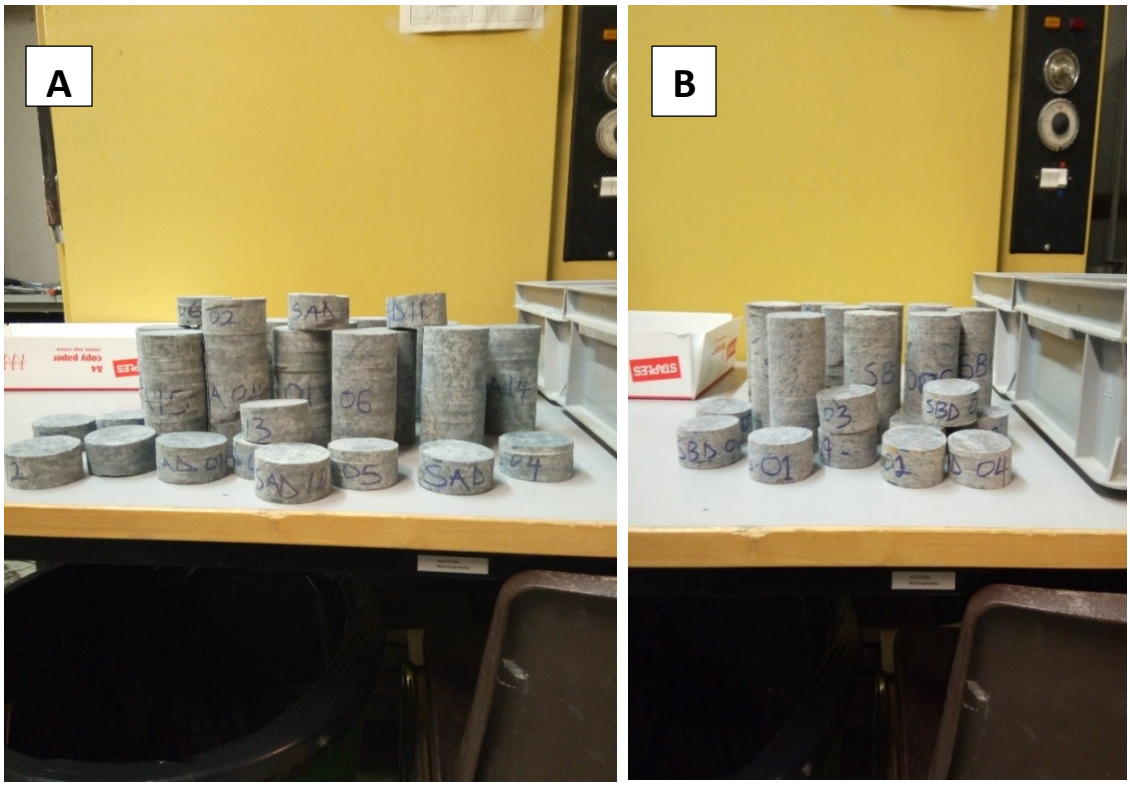

Figure 3.3. Cylindrical and disc shaped test specimens of (A) gabbro (B) granite

Figure 3.4. Cylindrical uniaxial compression test specimens after re-grinding (photographed by P. Eloranta, Aalto ENG)

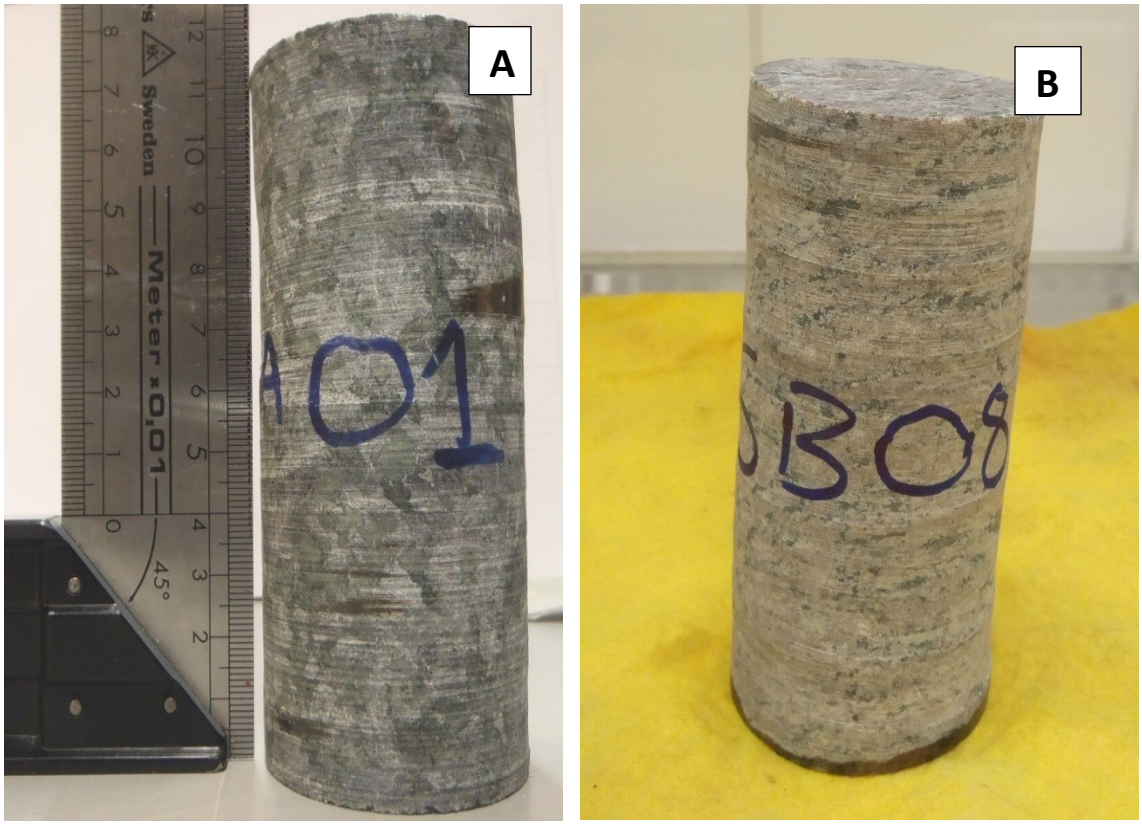

Figure 3.5. (A) specimen SA01 gabbro having ends not perpendicular to the axis (photographed by P. Eloranta, Aalto ENG) (B) specimen SB08 granite having uneven circumference

3.2 TEST PROCEDURES AND CONFIGURATIONS

3.2.1 EQUIPMENT

The UCS and Brazilian tests were conducted at Aalto University School of engineering. The MTS 815 Rock Mechanics Test System, a computer servo-controlled hydraulic compression machine was used (figure 3.6). The system consists of a load cell, extensometers for strain measurements, load frame, hydraulic power supply, test controller, test processor and PC micro-computer.

Figure 3.6. MTS 815 Rock mechanics test system

3.2.2 UCS, YOUNG'S MODULUS AND POISSON'S RATIO TESTS

In all UCS tests on the gabbro and granite specimens, axial deformation is measured with the three averaging direct contact extensometers which are 50.0 mm gauge length (figure 3.7). The extensometers are held in place by the contact force provided from six mounting springs. Circumferential deformation is measured by means of an extensometer connected to a roller chain wrapped around the circumference of the specimen at its mid-height. The axial load is applied to the top end through a spherical seat in order to assure uniform load distribution. Load is derived from the hydraulic pressure on the loading piston. Non-lubricated steel plates, fixed at the bottom and with spherical seat on top, are used for the UCS tests.

A detailed testing routine that conforms to ASTM D7012 (2014) and ISRM suggested methods (Ulusay and Hudson, 2007). The UCS tests are started under the axial deformation control and then switched to the circumferential deformation control at 0.75 MPa/s to ensure a controlled test in the post-peak region All measured data were recorded at a frequency of 1 Hz. The test procedure is listed below:

i) The specimen was driven manually near to contact (no axial force is allowed)
ii) The readings of the axial and radial extensometers, actuator displacement and axial force are reset.
iii) Programmed test control is initiated.
iv) The specimen is driven to force contact by moving actuator up to 0.2mm/min until axial force is 5.0KN
v) Axial load is increased so that loading rate is about 0.75MPa/s until radial strain is -0.01% or axial stress is 50Mpa. This is to ensure axial load ramp to failure.
vi) The system is unloaded by removing remaining force through programmed control

To ensure that all the test phases are made to each specimen in planned order, and to make possible and reanalyze possible errors and deviations in the test results, the test phases were reported on a test information form stored in the laboratory.

The UCS of the specimens is calculated according to ISRM, 2007 using equation (4). Eleven specimens were tested for Young's modulus and Poisson's ratio comprising five gabbro specimens and six granite specimens. Young's modulus (E) and Poisson's ratio

are calculated as tangent modulus at the half of the peak strength. The slopes of the stress-strain curves are determined between 40-60% of the peak strength using linear fit (Microsoft Excel SLOPE function) which corresponds with equations (7) and (8). Young's modulus is additionally calculated as secant modulus at half of the peak strength. Table 3.1 shows the results of the UCS, Young's modulus and Poisson's ratio tests.

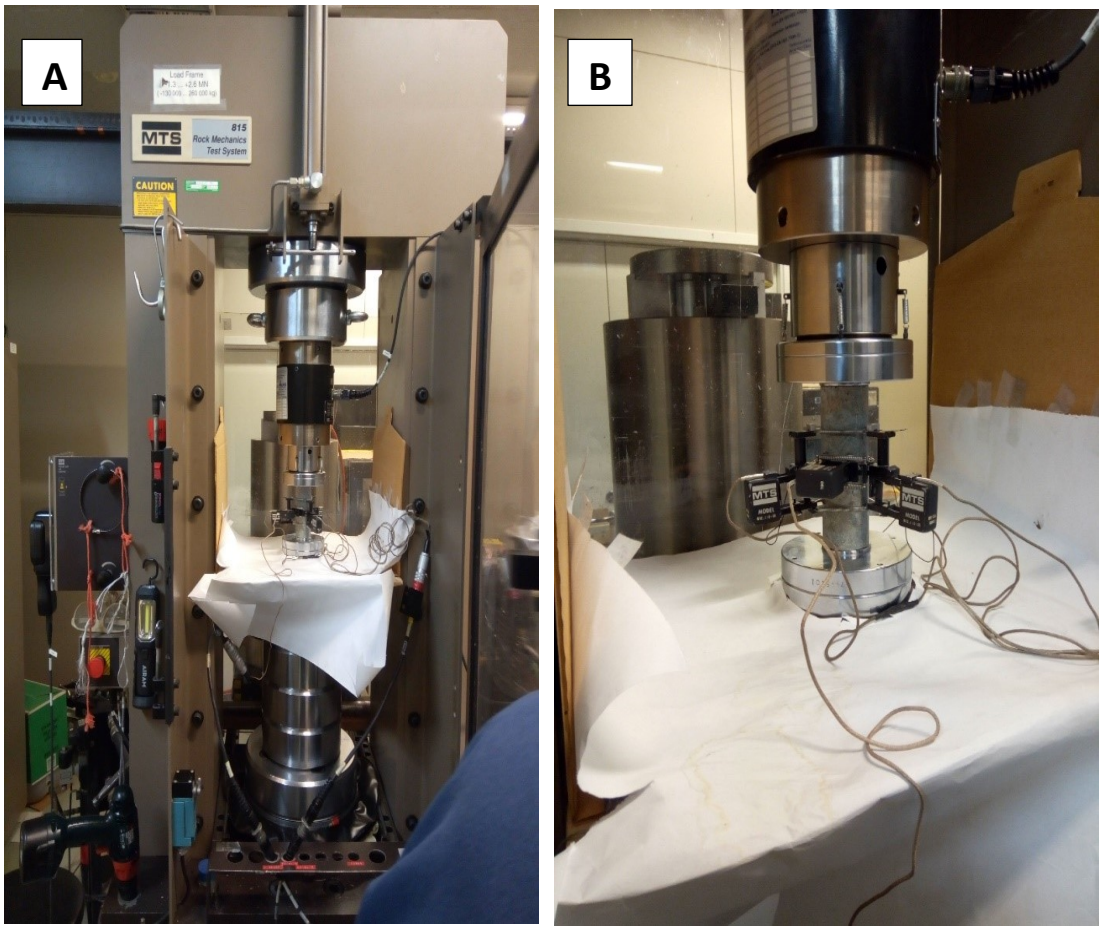

Figure 3.7 (A and B) Cylindrical specimen held by extensometers for UCS, Young's modulus and Poisson's ratio testing

3.2.3 BTS TESTING PROCEDURE

The BTS was conducted in accordance with the ISRM 2007 suggested method with 15 specimens for the gabbro and 10 for the granite. All 25 specimens were wrapped with a masking tape before the conduct of tests (Fig. 3.8).

The BTS tests are conducted under monotonically increasing load until the specimen failed. A testing routine that conforms to ASTM D3967 (2008b) is used and is detailed below:

i) The specimens were placed in the center of the curved bearing blocks or platens to contact the top platen.
ii) The readings of axial force were reset.
iii) The programmed test control routine is started.
iv) With the specimen in contact with the top platen,
    a. the actuator is moved up with the rate of 0.1 mm/min
    b. this is stopped when the applied force reaches 5.0 kN
    c. the applied force to the specimen is reduced to 1.0 kN with the unloading rate of 10 kN/min.
v) The applied force and lateral deformations are recorded.
vi) The test in load control mode with the rate ranging between 0.1 to 0.25 kN/s depending on the diameter of the specimen is started.
vii) When the applied force to the specimen in the unloading region reaches 60% of the maximum applied force to the specimen, the test is stopped.

The BTS of the specimens are calculated based on ISRM, 2007 equation (5). Table 3.1 shows results of the test.

Figure 3.8. A specimen wrapped with a masking tape for BTS test.

3.2.4 DENSITY, POROSITY AND WATER CONTENT MEASUREMENTS

The density of the specimens is calculated after preparation but before testing with the moisture content corresponding to the relative humidity of the room, according to the equations in ISRM (2007).

Density and Porosity: A VWR international's (American company involved in the distribution of research laboratory products) forced air oven capable of heating up to 105ºC, a vacuum saturation equipment, a dessicator to hold specimens during cooling, an immersion bath and a wire basket and a mass balance capable of weighing up to a sample weight accuracy of 0.01% were utilized in the testing. The procedure for the testing is listed as follows:

i) Representative crushed samples of the gabbro and granite having either a mass of at least 50 g or a minimum dimension of ten times the maximum grain size is selected. The samples are washed in water to remove dust.
ii) The granite samples are saturated by water immersion in a vacuum of less than 800 Pa for a period of at least one hour, with periodic agitation to remove trapped air.
iii) The sample were then transferred under water to the basket in the immersion bath. Its saturated-sub- merged mass M_{sub} was determined to an accuracy of 0.1 g from the difference between the saturated-submerged mass of the basket plus sample and that of the basket alone.
iv) The sample container with its lid is cleaned, dried and its mass (A) is determined.
v) The sample is removed from the immersion bath and surface-dried with a moist cloth, care being taken to remove only surface water and to ensure that no rock fragments are lost. The sample is transferred to the sample container, the lid replaced, and the mass (B) of saturated-surface-dry sample plus container is determined.
vi) The lid is removed, and the sample dried to constant mass at a temperature of 105°C, the lid replaced. The sample was allowed to cool for 30 min in a dessicator. The mass (C) of oven-dry sample plus container is measured.
vii) Steps (ii –vi) is repeated with the gabbro.

The parameters for the calculation of porosity and density are determined utilizing the equations (9-14). Table 3.1 shows results of the test conducted.

Water content: An VWR forced air oven capable of heating up to 105ºC, an air tight container with lid, a dessicator for holding samples during cooling and a mass balance capable of weighing up to a sample weight accuracy of 0.01% were utilized in the testing. The procedure for the testing is listed as follows:

i) The container with its lid is cleaned, dried and its mass (A) is determined.
ii) Representative crushed samples of the isotropic gabbro and gneissic granite having either a mass of at least 50 g or a minimum dimension of ten times the

maximum grain size is selected. Storage and handling precautions were adhered in order that, the water content remains within 1% of the in-situ value.

iii) The gabbro samples were placed in the container, the lid replaced and the mass (B) of sample plus container determined.

iv) The lid was removed, and the sample dried to constant mass at a temperature of 105°C.

v) The lid is replaced, and the sample allowed to cool in the dessicator for 30 min. the mass (C) of the sample together with the container is determined.

vi) Steps (iii – v) was applied with regards the water content determination for the granite

The water content is calculated from equation (17). Table 3.1 shows results of the test conducted.

3.2.5 THIN SECTION PREPARATIONS AND XRF ANALYSIS

Polished thin sections were prepared to study the mineralogy and textural characteristics of the rocks. The thin sections were examined using a petrographic microscope with transmitted and reflected light capabilities at the University of Oulu. The gabbro shows an isotropic and coarse-grained texture and is composed of euhedral laths of calcic plagioclase with interstitial spaces filled by clinopyroxene, which is replaced by amphibole. The granite shows fine to medium grained texture and consists of equigranular framework of quartz and alkali feldspar and dark coloured bands of amphibole, which define gneissic banding. Figure 3.9 shows microphotographs of the specimen slides in plain and crossed polarized transmitted light. Summary of the mineralogical and textural characteristics of the samples are shown in Table 3.2. In addition, chemical compositions of the rock types (Table 3.3) were determined by x-ray fluorescence analysis using pressed powder pellets and the Bruker AXS S4 spectrometer at the Center for Material Analysis (University of Oulu).

3.2.6 REGRESSION ANALYSIS

Multiple linear regression analysis was carried out using IBM SPSS Amos 25 statistics software suite. In the conduct of the linear regression test, the experimental results in Table (3.1) was grouped into two for the gabbro specimens and the granite specimens. The mean and mode of the Young's modulus and Poisson's ratio data respectively were used to complement for the unavailable data to carry out the regression tests. The statistical data of the rock properties representing the two rock types are shown in Table 3.4. Analysis of variance (ANOVA) technique was used to find out which relationship was statistically significant according to t-test, $p \leq 0.05$ and a 95% confidence level.

The general purpose of multiple regression was to learn more about the relationship between several predictor variables and a dependent or criterion variable. The performance of the model depends on a large number of factors that act and interact in a complex manner. The mathematical models of Poisson's ratio and Young's modulus (properties that had unavailable data in the experimental test) as well as UCS were primarily the target in order to facilitate future predictions with respect of the other rock properties. This turned out to be influenced by many factors, therefore, a detailed process representation anticipated a second order model.

Analysis of variance (ANOVA) technique was used to find out which input parameter significantly affects the desired response. Tables (3.5-3.9) shows the results for multiple regression tests run for the gabbro. Table 3.9 shows the regression statistics of the models generated. Model 1 represents prediction model for UCS, model 2 for Young's modulus and model 3 for Poisson's ratio. Some obtained relationships were found not to be statistically significant according to the t-test at 95% level of confidence. Multiple regression model to predict the relationship of various rock properties are presented in equations (33-38). Multiple regression models for the granite was statistically insignificant (Table 3.10).

3.2.7 ARTIFICIAL NEURAL NETWORK (ANN)

Multi-layer perceptron (MLP) containing a (4 x (14 x 3) x 3) architecture was used in this study. This structure means that the ANN has three layers, 4 neurons in the input representing (BTS, density, porosity, water content), two hidden layesr containing 14 neurons in layer 1 and 3 neurons in layer 2, and 3 output neurons, representing (UCS, Young's modulus and Poisson's ratio). Two hidden layers were utilized, with Logsigmoid function chosen as the activation function in layer 1 and a linear function in layer 2. Figure 3.10 shows a Simulink model of the network architecture.

This architecture was chosen to facilitate prediction of the output parameters of the specimens that had unavailable data for Young's modulus and Poisson's ratio and UCS due to specimens not meeting standardized sample preparation criteria. Eighteen datasets representing eleven for the gabbro and seven for the granite were run through this analysis. Matlab R2019a was the software suite used for this analysis.

In this study, the nnstart command in matlab was utilized in the development of the model. The inputs (BTS, density, porosity, water content) and targets (UCS, Young's modulus, Poisson's ratio) were sampled from 70% of the datasets to train the network as recommended by (Haykin, 1999). The testing was done with 15% and another 15% for validation using the Levenberg– Marquardt algorithm (trainlm) for training the network. A few trials were conducted initially to fix the number of neurons in the hidden layer. The number of neurons for which (mean squared error) MSE is minimum was selected as the optimum number of neurons in the hidden layer. The output of the network was compared with the target output at each presentation and the error was computed. The initial weights and biases of the network were fixed randomly.

Four models were generated with this network architecture, stopping the model when the MSE was small. These models are evaluated with performance prediction indices of root mean square (RMSE), variance accounted for (VAF) and the coefficient of correlation ($R^{2)}$ to select the best model for prediction. The basic philosophy of the ranking procedure proposed by (Zorlu et al., 2008) was considered and the ranking values of each dataset were calculated for each model separately. Table 3.11 shows the input data for the training of the network. In Table 3.12, the output data for the models, indicating the training and

testing data for the respective models are presented. Table 3.13 shows the performance prediction indices of the models and their rankings, respectively. Figures (3.11- 3.14) show the regression chart for the models and figures (3.15-3.18), the error histogram of the models.

3.3 TEST RESULTS AND DATA

In this work, petrographic and XRF analysis are presented and explanations sought to link their influence on other rock strength. Also, regression and ANN models are formulated, and their prediction capacities are analyzed. The obtained VAF and RMSE values are also presented.

3.3.1 MECHANICAL AND PHYSICAL PROPERTIES

Table 3.1 Test results for mechanical and physical properties of the rock specimens

SAMPLE ID	UCS (Mpa)	BRAZILIAN TEST (Mpa)	YOUNG'S MODULUS (Gpa)	POISSON'S RATIO	DENSITY (Kg/m³)	POROSITY (%)	WATER CONTENT (%)
SA01	226	12.3			2852	0.3	0.03
SA02*	294	11.4	104	0.28	2856	0.2	0.02
SA03*	303	8.9	103	0.29	2890	0.28	0.02
SA04	133	9			2887	0.48	0.04
SA05	76	8.6			2922	0.26	0.02
SA06*	299	8.3	108	0.28	2960	0.4	0.04
SA07	97	12.3			2875	0.22	0.01
SA08*	295	10.6	106	0.25	2768	0.22	0.01

SA09	125	9.2			2964	0.38	0.02
SA10	106	11.8			2953	0.19	0.01
SA11	116	10.5			2972	0.24	0.01
SA12*	303	9.7	105	0.29	2954	0.13	0.01
SA13	78	6.8			2876	0.26	0.01
SA14	100	11.2			2880	0.43	0.02
SA15	91	7.3			2871	0.39	0.01
SB01	97	12.7			2688	1.64	0.12
SB02*	275	12.5	70	0.29	2688	1.18	0.11
SB03*	284	10	71	0.29	2689	0.77	0.04
SB04	141	9.4			2699	0.37	0.02
SB05*	228	7.3	65	0.28	2696	0.29	0.02
SB06*	242	7.1	65	0.27	2690	0.42	0.03
SB07*	231	11.2	65	0.27	2676	0.55	0.04
SB08	184	11.1			2673	0.79	0.06
SB09	68	11.1			2688	0.96	0.05
SB10*	258	11.7	64	0.28	2683	0.37	0.03

SA (01-15) = gabbro, SB (01-10) = granite (_*) Standardized sample

3.3.2 PETROGRAPHY AND XRF ANALYIS

Table 3.2. Mineralogical characteristics of gabbro and granite

ROCK	MINERALS	MINERAL (%)	GRAIN SIZE (mm)
GABBRO	Clino-pyroxene	47	2-5
	Plagioclase	43	2-4
	Hornblende	5	0.5-1
	Opaque minerals	2	0.5-1
	Other minerals	3	0.5-1
GRANITE	Alkali/ K-feldspars	50	0.5-2
	Quartz	32	0.1-1
	Amphibole	10	0.1-0.5
	Opaque minerals	5	1-1.5
	Other minerals	3	0.5-1

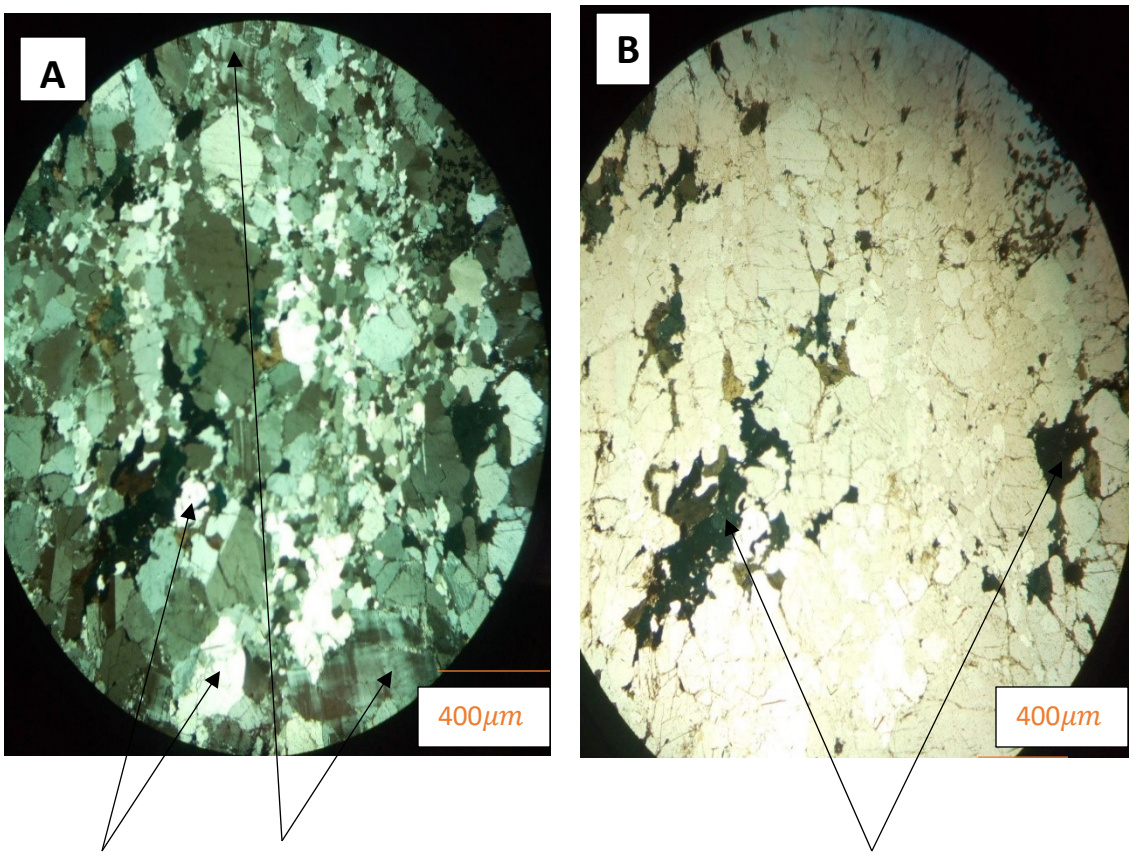

Quartz K-feldspar exhibiting (cross-hatched twinning) Amphiboles

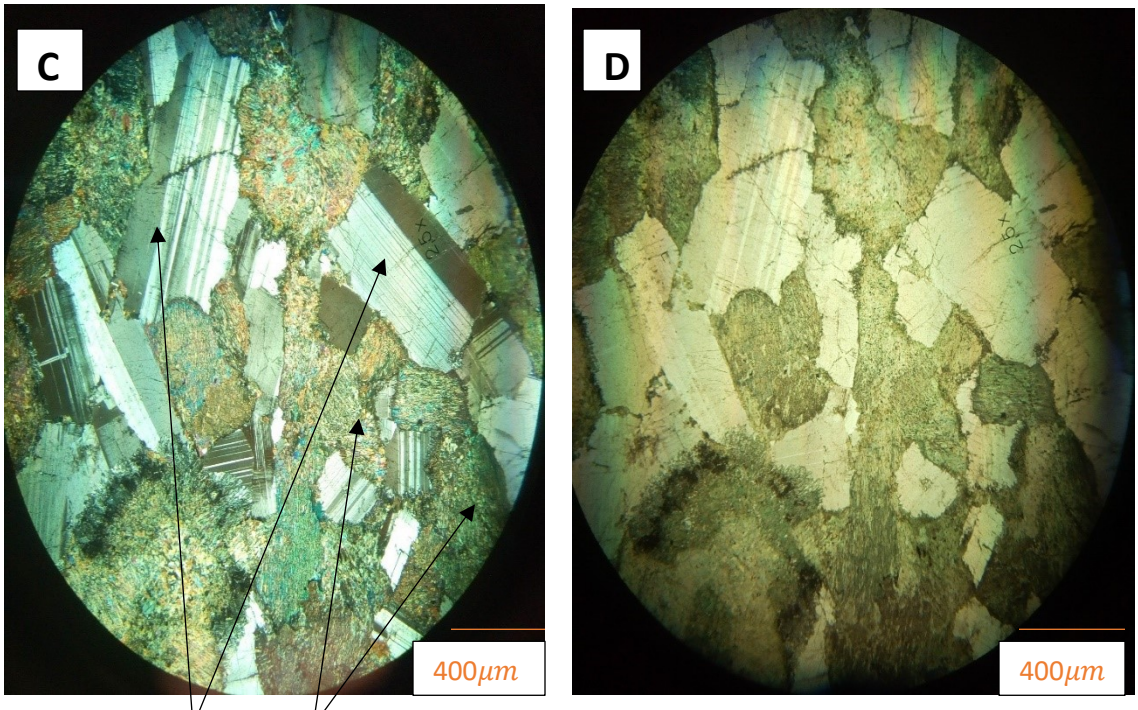

Plagioclase Clino pyroxene (altered to fine-grained hornblende)

Figure 3.9. Microphotomicrographs of granite and gabbro samples from polished thin sections A-D (A) gneissic granite (crossed polarized light) with alkali feldspars exhibiting crosshatched twinning interspersed with subhedral quartz grains; (B) gneissic granite (plane polarized light); (C) isotropic gabbro (crossed polarized light) composed of plagioclase with characteristics carlsbard twinning and twin lamellae, clino pyroxene altered to fine-grained hornblende; (D) isotropic gabbro (plane polarized light).

The matrix of the granite is characterized by subhedral to anhedral alkali-feldspars (potassium feldspar and albite), subhedral to anhedral quartz grains and anhedral amphibole grains (Fig 3.9 A and B). The alkali-feldspars are brownish-grey, have fractures, exhibit cross-hatched twinning occasionally with straight to sinuous grain boundaries with quartz. Quartz is deformed and exhibits large variations in grain size. The amphibole mineral grains were conspicuous as dark silicates in both plane and cross polars exhibiting sinuous contacts with the alkali-feldspars and the quartz. (fig. 3.9B).

The alkali-feldspars (~ 50 vol.%) and quartz (~ 30 vol.%) dominate the mode. These minerals, however, vary in terms of grain sizes with alkali-feldspars ranging from 0.5-2 mm and quartz with 0.1-1 mm value (Table 3.2).

The gabbro samples show isotropic texture (Fig. 3.9 C and D) and is composed of equidimensional euhedral plagioclase laths and subhedral clino-pyroxene, anhedral amphibole mineral grains. The plagioclase exhibited carlsbard twinning with twin lamellae, have coarse grains ranging between 2-4 mm in size with few visible fractures in the grains. The clino-pyroxene grains vary from 2 to 5 mm in size and exhibit cleavages with alteration along cracks in the crystal grains. These alterations were observed to be secondary hornblende, which has replaced primary clino pyroxenes probably after the magmatic crystallization. The grain boundary features between the clino-pyroxene and plagioclase are straight, but somewhat irregular due to growth of secondary hornblende. Minor opaque minerals occur as small anhedral to subhedral in clinopyroxene and amphibole.

The modal composition of the gabbro is dominated by clino-pyroxene (47 vol.%) and plagioclase (43 vol.%) as observed in Table 3.2. Modal grain size for these two minerals show coarse texture of about 3-3.5 mm.

Table 3.3. Major and Trace element compositions of the rock types in weight percent

	Gabbro			Granite		
	n	AC	SD	n	AC	SD
Na_2O	15	2.86	0.26	10	5	0.34
MgO	15	6.88	1.14	10	0.12	0.02
Al_2O_3	15	17.48	1.24	10	11.87	0.68
SiO_2	15	47.4	0.5	10	67.87	1.8
K_2O	15	0.26	0.04	10	4.31	0.22
CaO	15	12.42	0.44	10	0.46	0.12
FeO_{tot}	15	6.04	0.75	10	4.41	0.41
TiO_2	15	0.66	0.15	10	0.39	0.082
MnO	15	0.12	0.014	10	0.11	0.008
P_2O_5	15	0.04	0.01	10	0.04	0.01
Cl	15	0.03	0.011	10	0.02	0.014
S	15	0.09	0.031	6	0.031	0.03
F				7	0.109	0.042
Ni	15	0.016	0.002	9	0.007	0.007
Cu	15	0.013	0.009	9	0.012	0.022
Zn	15	0.006	0.001	10	0.012	0.004
Ga	15	0.001	0.001	10	0.002	0.005
Sr	15	0.069	0.005	10	0.019	0.026
Ba	15	0.011	0.001	9	0.01	0.003
Y	1	0.001	0	7	0.011	0.004
Zr				7	0.107	0.052
Nb				7	0.017	0.011
Ce				9	0.02	0.013
Nd				6	0.015	0.01
Pb				2	0.005	0.002
Th				5	0.034	0.002
Cr	15	0.026	0.004	3	0.031	0.001
Hf				1	0.004	0
Rb				7	0.017	0.001
Ta	1	0.003	0			

SD = standard deviation, AC = average composition, n = number of samples

3.3.3 REGRESSION ANALYSIS

Table 3.4 Statistical values of rock properties for the regression analysis

Rock type	Statistical parameter	UCS (Mpa)	BTS (Mpa)	Younng's modulus (GPa)	Poisson's ratio	Density (kg/m³)	Porosity (%)	Water content (%)
Gabbro	Number of data	15	15	15	15	15	15	15
	Minimum value	76	6.8	103	0.25	2768	0.13	0.01
	Maximum value	303	12.3	108	0.29	2972	0.48	0.04
	Range	227	5.5	5	0.04	204	0.35	0.03
	Mean	176.13	9.68	105.07	0.2799	2898.67	0.292	0.0187
	Standard deviation	96.27	1.75	10.3	0.00884	55.7	0.10136	0.0106
Granite	Number of data	10	10	10	10	10	10	10
	Minimum value	68	7.1	64	0.27	2673	0.29	0.02
	Maximum value	284	12.7	71	0.28	2699	1.64	0.12
	Range	216	5.6	7	0.01	26	1.35	0.1
	Mean	200.8	10.41	66.8	0.28	2687	0.734	0.052
	Standard deviation	75.511	1.96	2.25	0.00667	7.986	0.431	0.03553

GABBRO

Model 1 (UCS) = $1770.51 - 7.82_{BTS} - 0.49_{density} - 822.52_{porosity} + 75773.86_{water\ content}$ (33)

Model 2 (Young's modulus) = $99.75 - 0.05_{BTS} + 0.002_{density} + 0.14_{porosity} + 30.07_{waer\ content}$ (34)

Model 3 (Poisson's ratio) = $0.001 - 0.0004_{BTS} + 0.0001_{density} - 0.0086_{porosiity} + 0.12_{water\ content}$ (35)

Table 3.5. Analysis of variance for model 1

ANOVA[a]

Model 1	Sum of Squares	df	Mean Square	F	Sig.
Regression	62319.095	4	15579.77	2.309872	0.129[b]
Residual	67448.638	10	6744.864		
Total	129767.73	14			

a. Dependent Variable: UCS (Mpa)

b. Predictors: (Constant), WATER CONTENT (%), DENSITY (Kg/m³), BRAZILIAN TEST (Mpa), POROSITY (%)

Table 3.6. Analysis of variance for model 3

ANOVAa

Model		Sum of Squares	df	Mean Square	F	Sig.
1	Regression	0.000458	4	0.000114516	1.802628	0.205b
	Residual	0.000635	10	6.35271E-05		
	Total	0.001093	14			

a. Dependent Variable: POISSON'S RATIO

b. Predictors: (Constant), WATER CONTENT (%), DENSITY (Kg/m³), BRAZILIAN TEST (Mpa), POROSITY (%)

Table 3.7. Correlation coefficients of the relation amongst the independent variables for model 1

		UCS (Mpa)	BRAZILIAN TEST (Mpa)	DENSITY (Kg/m³)	POROSITY (%)	WATER CONTENT (%)
Pearson Correlation	UCS (Mpa)	1	0.1285	-0.1992	-0.2704	0.2493
	BRAZILIAN TEST (Mpa)	0.1285	1	-0.1651	-0.3467	-0.0917
	DENSITY (Kg/m³)	-0.1992	-0.1651	1	0.0167	0.0899
	POROSITY (%)	-0.2704	-0.3467	0.0167	1	0.6607
	WATER CONTENT (%)	0.2493	-0.0917	0.0899	0.6607	1

Table 3.8. Correlation coefficients of the relation amongst the independent variables for model 3

		POISSON'S RATIO	BRAZILIAN TEST (Mpa)	DENSITY (Kg/m³)	POROSITY (%)	WATER CONTENT (%)
Pearson Correlation	POISSON'S RATIO	1	-0.1543	0.6365	0.0335	0.1423
	BRAZILIAN TEST (Mpa)	-0.1543	1	-0.1651	-0.3467	-0.0197
	DENSITY (Kg/m³)	0.6365	-0.1651	1	0.0167	0.0899
	POROSITY (%)	0.0335	-0.3467	0.0167	1	0.6607
	WATER CONTENT (%)	0.1423	-0.0197	0.0899	0.6607	1

Table 3.9. Statistics results of the regression models

	INDEPENDENT VARIABLES	LINEAR COEFFICIENTS	STANDARD ERROR	t-VALUE	p-VALUE
MODEL 1	CONSTANT	1770.515	1214.62	1.458	0.176
	BTS	-7.817	13.905	-0.562	0.586
	DENSITY	-0.489	0.404	-1.211	0.254
	POROSITY	-822.517	314.912	-2.612	0.026
	WATER CONTENT	7573.861	2841.763	-2.665	0.024
MODEL 2	CONSTANT	99.75	16.824	5.929	0.00014
	BTS	-0.054	0.1925	-0.281	0.7848
	DENSITY	0.0018	0.0056	0.323	0.753
	POROSITY	0.1408	4.362	0.0323	0.9749
	WATER CONTENT	30.065	39.3622	0.7638	0.4626
MODEL 3	CONSTANT	0.00104	0.1179	0.0119	0.9907
	BTS	-0.00037	0.00135	-0.2769	0.7875
	DENSITY	0.0001	3.90E-05	2.4796	0.0326
	POROSITY	-0.00859	0.0305	-0.2812	0.7843
	WATER CONTENT	0.1214	0.2758	0.44	0.6693

GRANITE

Model 1 (UCS) = $4440.1 - 5.86_{BTS} - 1.53_{density} - 315.75_{porosity} + 3325.74_{water\ content}$ (36)

Model 2 (Young's modulus) = $-117.72 + 0.10_{BTS} + 0.07_{density} + 3.61_{porosity} - 13.81_{water\ content}$ (37)

Model 3 (Poisson's ratio) = $-0{,}91 + 0.002_{BTS} + 0.001_{density} - 0.001_{poroosity} + 0.027_{water\ content}$ (38)

Table 3.10. Statistics results of the regression models for granite

	INDEPENDENT VARIABLES	LINEAR COEFFICIENTS	STANDARD ERROR	t-VALUE	p-VALUE
MODEL 1	CONSTANT	4440.078	10251.712	0.433	0.683
	BTS	-5.859	21.698	-0.270	0.798
	DENSITY	-1.534	3.778	-0.406	0.702
	POROSITY	-315.749	180.325	-1.751	0.140
	WATER CONTENT	3325.739	2203.936	1.509	0.192
MODEL 2	CONSTANT	-117.721	341.588	-0.345	0.744
	BTS	0.1034	0.723	0.143	0.892
	DENSITY	0.068	0.126	0.537	0.615
	POROSITY	3.611	6.008	0.601	0.574
	WATER CONTENT	-13.806	73.435	-0.188	0.858
MODEL 3	CONSTANT	-0.909	0.987	-0.921	0.399
	BTS	0.002	0.002	0.900	0.410
	DENSITY	0.001	0.001	1.196	0.285
	POROSITY	-0.001	0.017	-0.054	0.959
	WATER CONTENT	0.0265	0.212	0.125	0.905

3.3.4 ARTIFICIAL NEURAL NETWORK (ANN)

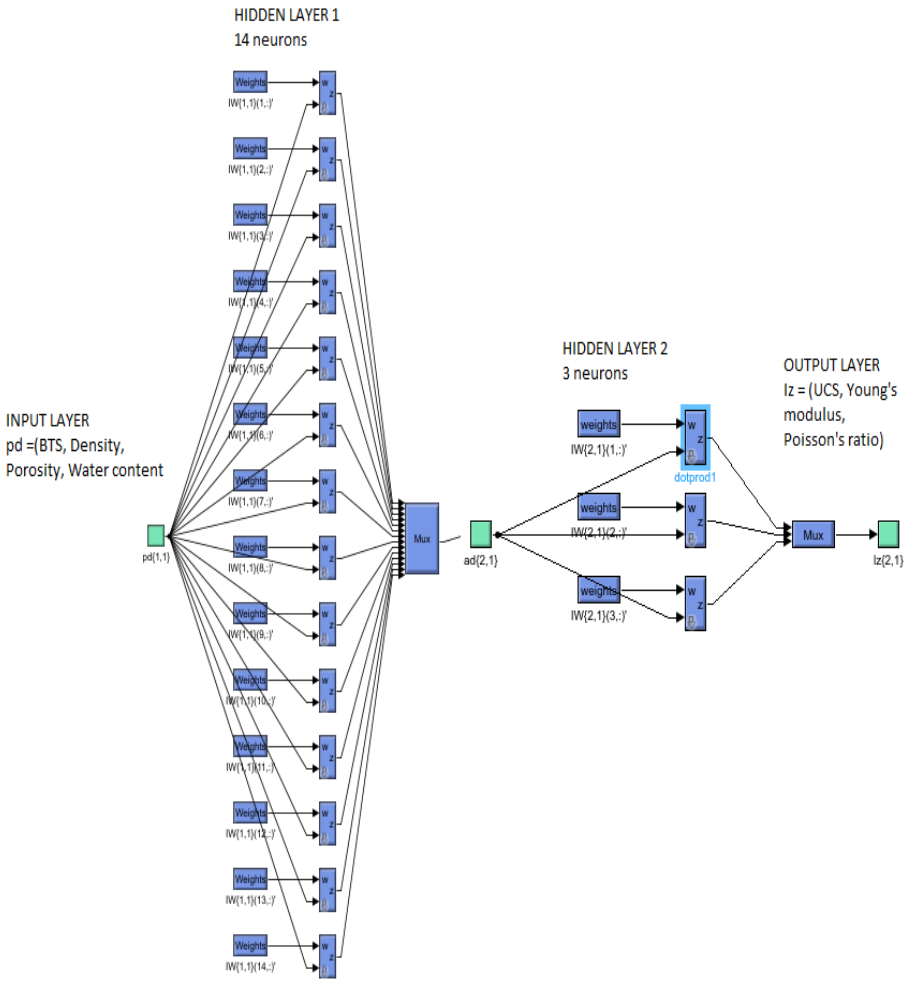

Figure 3.10. Simulink model of the network architecture

Table 3.11 Matlab ANN training data

INPUT DATA				OUTPUT DATA		
BTS	Density	Porosity	Water ctnt	UCS	Young's mdls	Poisson's ratio
12.3	2852	0.3	0.03	226	105	0.28
11.4	2856	0.2	0.02	294	104	0.28
9	2887	0.48	0.04	133	105	0.28
10.6	2768	0.22	0.01	295	106	0.25
9.2	2964	0.38	0.02	125	105	0.28
10.5	2972	0.24	0.01	116	105	0.28
12.5	2688	1.18	0.12	275	70	0.29
10	2689	0.77	0.04	284	71	0.29
7.1	2690	0.42	0.03	242	65	0.27
11.2	2676	0.55	0.04	231	65	0.27
11.7	2683	0.37	0.03	258	64	0.28
8.9	2890	0.28	0.02	303	103	0.29
11.8	2953	0.19	0.01	106	105	0.28
9.7	2954	0.13	0.01	303	105	0.29
7.3	2696	0.29	0.02	228	65	0.28
8.3	2960	0.4	0.04	299	108	0.28
11.1	2673	0.79	0.06	184	105	0.28

Water ctnt = water content, Young's mdls = Young's modulus

Table 3.12 ANN output data for the models

	Ttrain			Ytrain		
MODEL 1	UCS	Young's modulus	Porosity	UCS	Young's modulus	Porosity
	226	105	0.28	177.5848	99.43089	0.285413
	294	104	0.28	248.2675	105.005	0.284703
	133	105	0.28	166.6354	102.9148	0.26379
	106	105	0.28	116.8805	108.7742	0.274398
	116	105	0.28	97.26253	111.4294	0.257539
	303	105	0.29	236.4533	104.2939	0.252087
	275	70	0.29	289.6375	75.10485	0.314534
	284	71	0.29	309.3419	62.55101	0.298555
	242	65	0.27	355.6054	46.95317	0.278071
	231	65	0.27	242.137	60.05656	0.285202
	258	64	0.28	260.7225	58.8735	0.280506
		Ttest			Ytest	
	299	108	0.28	44.56497	104.7977	0.259831
	125	105	0.28	73.91798	110.5915	0.250885
	228	65	0.28	428.1996	53.69923	0.267691
MODEL 2		Ttrain			Ytrain	
	226	105	0.28	225.7998	104.9944	0.279048
	294	104	0.28	293.985	103.9853	0.281884
	303	103	0.29	302.8979	102.9344	0.282315
	295	106	0.25	295.2023	105.9974	0.282384
	125	105	0.28	124.4595	104.6841	0.278465
	106	105	0.28	105.7925	104.9124	0.277144
	116	105	0.28	114.9928	104.858	0.277855
	228	65	0.28	227.553	64.97697	0.269585
	242	65	0.27	242.014	65.06133	0.269149
	184	67	0.28	183.3393	67.1551	0.25796
	258	64	0.28	258.1549	63.99556	0.279047
		Ttest			Ytest	
	133	105	0.28	133	105	0.28
	303	105	0.29	303	105	0.29
	284	71	0.29	284	71	0.29
MODEL 3		Ttrain			Ytrain	
	226	105	0.28	226.0001	105.0001	0.279999
	294	104	0.28	293.9999	104.0001	0.279999
	133	105	0.28	132.9999	104.9999	0.28
	299	108	0.28	298.9998	107.9998	0.28

	295	106	0.25	294.9998	106	0.25
	106	105	0.28	106.0007	105.0001	0.279999
	116	105	0.28	115.9996	105	0.279999
	275	70	0.29	274.9998	70	0.29
	228	65	0.28	228.0003	65	0.28
	184	67	0.28	184.0003	67.00006	0.28
	258	64	0.28	258.0002	64.0001	0.28
		Ttest			Ytest	
	303	105	0.29	278.762	112.2877	0.277763
	284	71	0.29	107.964	81.73808	0.262532
	231	65	0.27	194.1953	63.71488	0.279276
MODEL 4		Ttrain			Ytrain	
	226	105	0.28	148.5075	124.9799	0.283864
	294	104	0.28	173.4009	124.1604	0.281507
	133	105	0.28	160.4861	99.60045	0.274508
	299	108	0.28	229.9574	102.8672	0.272666
	295	106	0.25	228.7918	103.9818	0.273913
	116	105	0.28	115.0165	125.9362	0.283775
	303	105	0.29	192.2377	112.1041	0.280818
	275	70	0.29	265.2277	67.97289	0.271168
	284	71	0.29	221.6157	67.81167	0.270239
	184	67	0.28	180.0016	65.83988	0.277802
	258	64	0.28	264.1009	67.50909	0.268895
		Ttest			Ytest	
	106	105	0.28	119.9543	129.7582	0.284866
	228	65	0.28	359.6648	157.5121	0.264462
	231	65	0.27	227.364	65.95972	0.269681

Ttrain= target output for training data, Ttest= target output for testing data, Ytrain= model output for training, Ytest=model output for testing

Table 3.13. Performance prediction indices of the ANN models and their rankings

MODELS	ROCK PROPERTIES	RMSE	VAF	R^2	RATINGS			RANK VALUE
					RMSE	VAF	R^2	
Model 1	UCS Tr	47.05	53.99	0.53	2	2	3	7
	Tst	189.23	-577.57	-6.01	1	0	0	1

	Young's modulus Tr	7.17	87.54	0.85	3	3	3	9
	Tst	7.51	87.6	0.85	3	3	4	10
	Poisson's ratio Tr	0.017	-558.29	-0.098	1	0	0	1
	Tst	0.0224	0	0	5	0	0	5
								33
Model 2	UCS Tr	0.44	99.99	0.99	4	4	4	12
	Tst	0	100	1	5	5	5	15
	Young'smodulus Tr	0.122	99.99	0.99	4	5	4	13
	Tst	0	100	1	5	5	5	15
	Poisson's ratio Tr	0.012	-69.67	0.63	4	0	3	7
	Tst	0	100	1	5	5	5	15
								77
Model 3	UCS Tr	0.007	100	1	5	5	5	15
	Tst	104.77	-409.77	-10.82	2	0	0	2
	Young's modulus Tr	0.006	99.99	1	5	5	5	15
	Tst	7.523	91.76	0.81	4	4	3	11
	Poisson's ratio Tr	0.0007	99.73	0.997	5	5	5	15
	Tst	0.0129	-75	-0.875	2	0	0	2
								60
Model 4	UCS Tr	65.2	46.45	0.004	1	1	1	3
	Tst	79.46	-6.39	-0.72	4	0	0	4
	Young's modulus Tr	11.205	68.69	0.61	1	1	1	3
	Tst	55.29	-323.15	-7.59	1	0	0	1
	Poisson's ratio Tr	0.0122	-21.045	0.538	3	0	2	5
	Tst	0.0095	-225	-3.095	3	0	0	3
								19

Tr = training values, Tst = testing values

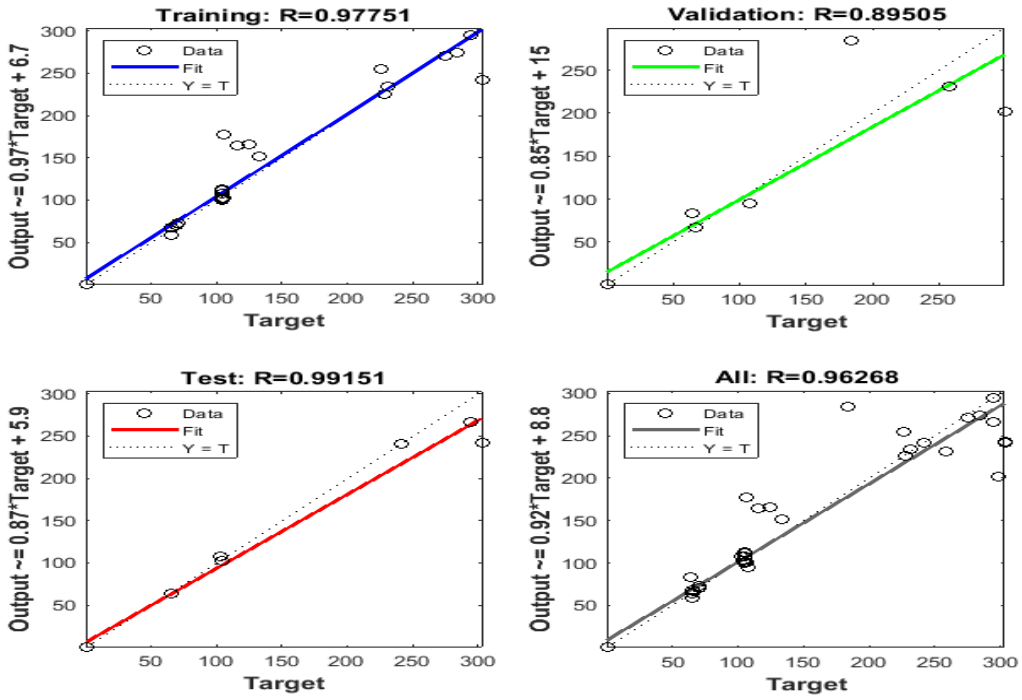

Figure 3.11. Regression chart for model 1

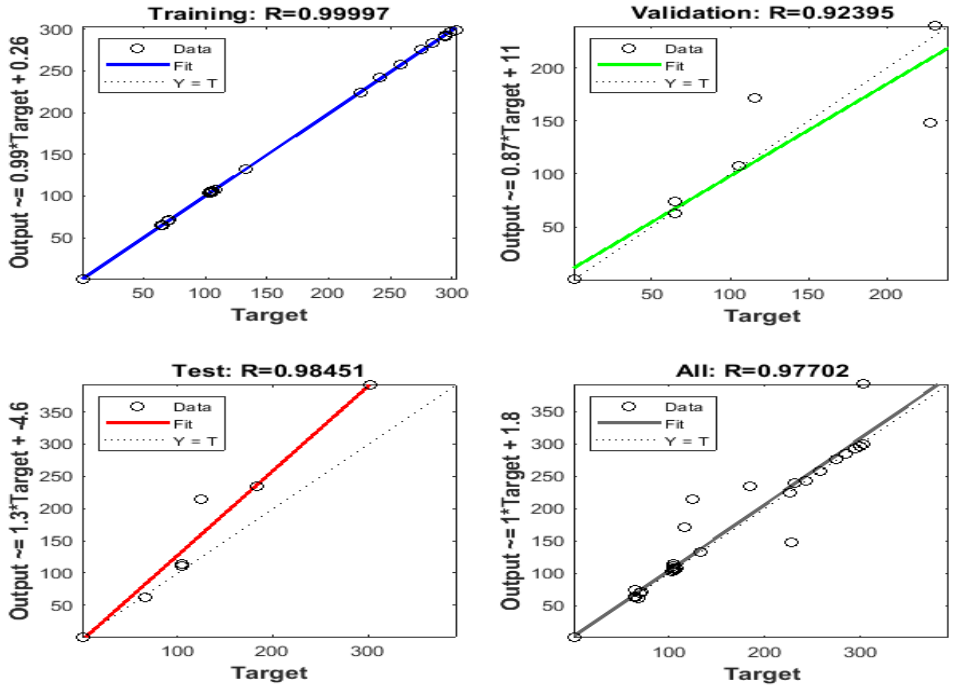

Figure 3.12. Regression chart for model 2

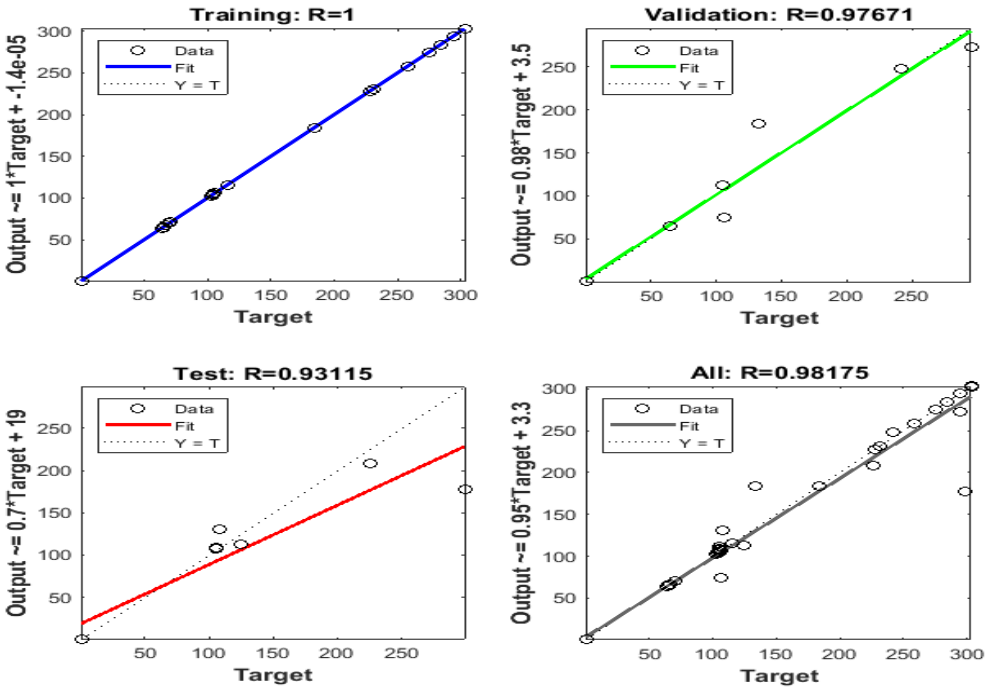

Figure 3.13. Regression chart for model 3

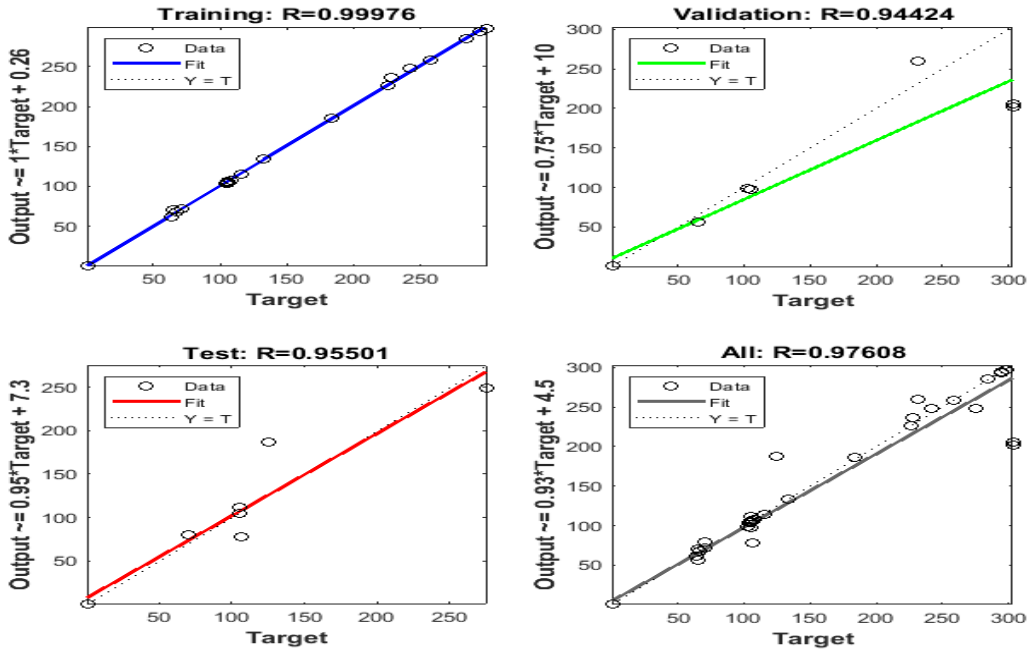

Figure 3.14. Regression chart for model 4

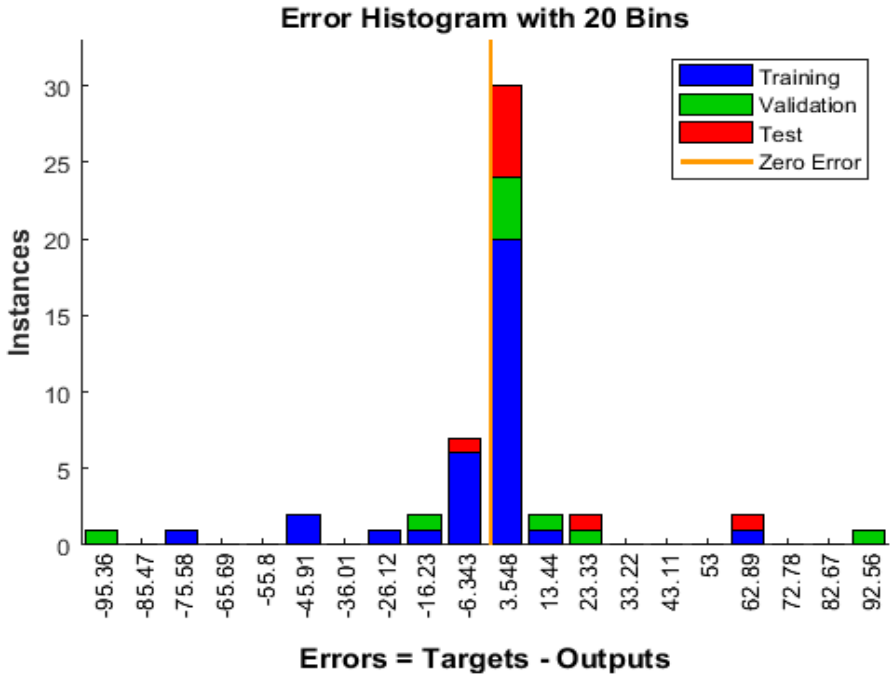

Figure 3.15. Error histogram for model 1

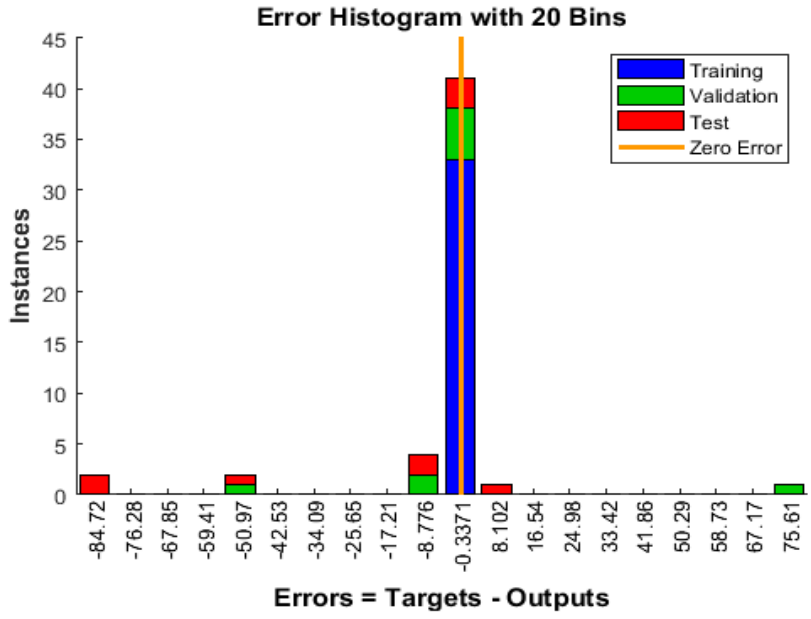

Figure 3.16. Error histogram for model 2

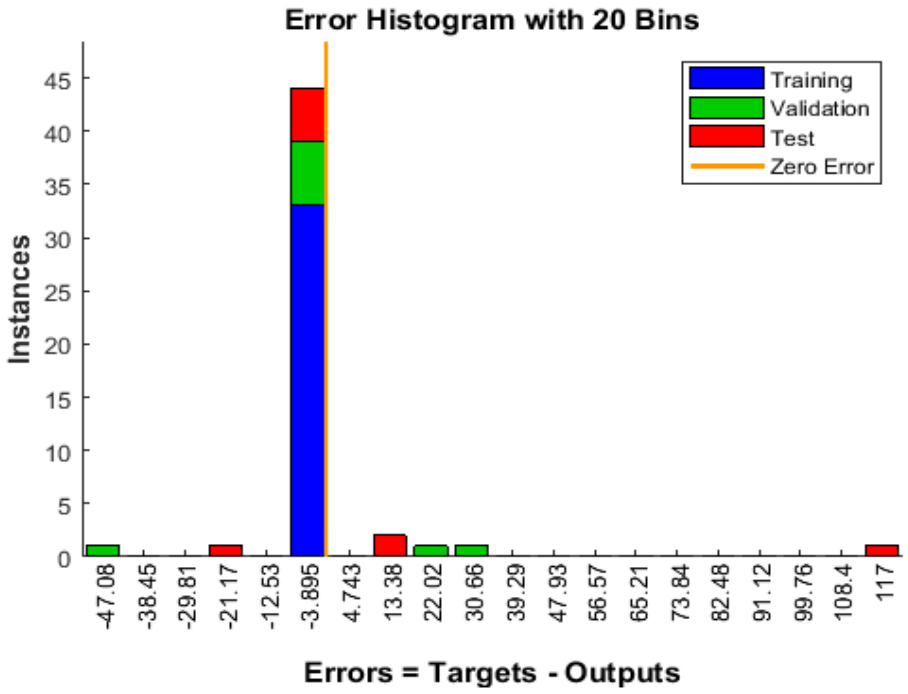

Figure 3.17. Error histogram for model 3

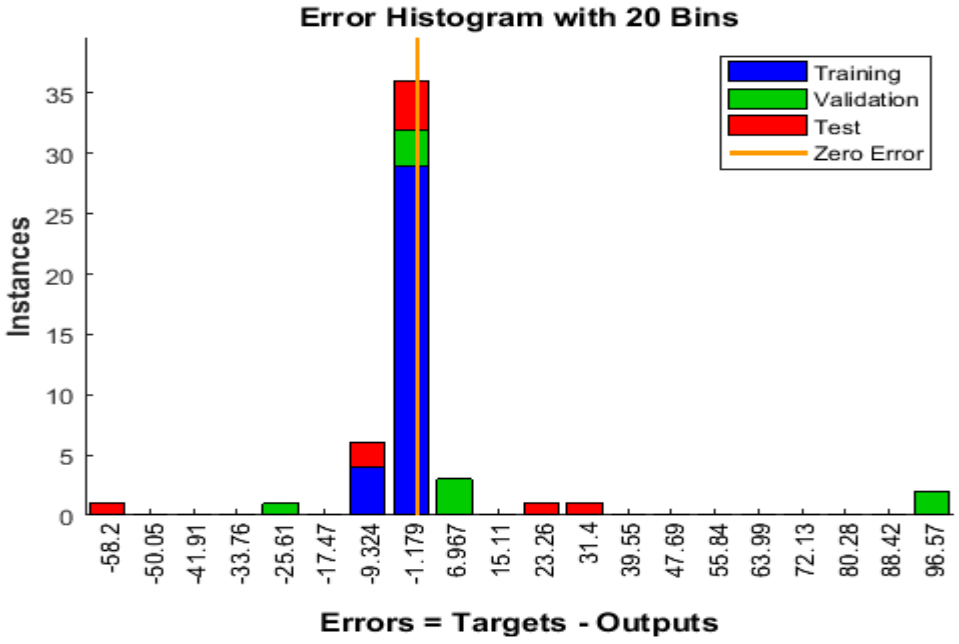

Figure 3.18. Error histogram for model 4

4 DISCUSSION

4.1 MECHANICAL AND PHYSICAL PROPERTIES TEST RESULTS

The UCS data from Table 3.1 shows great variation between specimens that met test standards and those that did not. Standardized gabbro specimens have an average 299 MPa as against 115 MPa for the non-standardized specimens. With the granite, the average UCS data for standardized specimens is 253 MPa as against 123 MPa for the non-standardized specimens. These variations show the effect of non-uniform stress distribution in the specimens during the testing process. Non flat ends will result in a concentration of stress in a plane not parallel to the axial force direction, inducing tensile stress at the ends of the specimens, hence resulting in a lower UCS value. Test result for Young's modulus and Poisson's ratio show quite consistent results with little variation.

The BTS test results from Table 3.1 range from 7.3-12.3 MPa for gabbro and 7.1-12.7 MPa for the granite. The variations could be explained as the effect of non-uniformity in the circumference of some specimens after the wrapping of the masking tapes for the conduct of the tests. As observed in figure 3.9(B), there were instances where specimens' circumference was not in uniform contact with the top plates of the test setup.

The average density from Table 3.1 for gabbro is 2899 kg/m^3. The porosities and corresponding water contents of the test specimens are relatively low. Specimens SA04 and SA06 however, have relatively high values of 0.48 and 0.40 wt% respectively with regards porosity which reflects in the high 0.04% water content values for both specimens.

The granite had an average density value of 2687 kg/m^3 and high porosity values relative to the gabbro. Specimens SB01 and SB02 have high values of 1.64 and 1.18 wt%. These high values had effects on the corresponding relatively high-water contents for these specimens as voids and/or cracks can leave openings to be filled by air and water.

4.2 PETROGRAPHY AND XRF ANALYSIS

4.2.1 PETROGRAPHY

Physico-mechanical properties depend on the petrographic characteristics (mineralogical composition, texture, size, shape and arrangement of mineral grains, nature of grains contact and degree of grain interlocking), alteration and deformation degree of the source rock (Smith and Collis, 2001; Miskovsky et al., 2004).

The mineral texture exhibited in by the granite is crystalline, thereby interlocking the grains to increase the response of the rock to applied stress, which will lead to a high UCS value. The average 253 MPa UCS value for granite affirms this. The opaque minerals are commonly included in the alkali-feldspar crystals. According to (Schneider, 1974), these inclusions are regions of resorption at the grain boundaries and are characterized by the replacement and intergrowths of alkali-feldspar with Fe-Ti oxides and quartz.

When grain size increases, there is more pore presence between the grains (Jin et al., 2018). This has the tendency to influence the strength of rock. However, the relatively high UCS values observed for the standardized gabbro specimens are a complete departure from this phenomenon with their relatively large grain size (Table 3.2). This could be due to the interlocking nature of its crystals. This means that, other factors such as mineral composition, degree of grain interlocking and low degree of alterations override the influence of larger grain size.

4.2.2 XRF ANALYSIS

XRF chemical analysis from Table 3.3 presents the average compositions by weight %, standard deviations of the major, minor and trace elements of the analyzed samples. Major elements were determined as oxides of (Na_2O, MgO, Al_2O_3, SiO_2, K_2O, CaO, FeO_{tot},TiO_2, MnO, P_2O_5) and trace elements (Cl. S, F, Ni, Cu, Zn, Ga, Sr, Ba, Y, Zr, Nb, Ce, N, Pb, Th, Cr, Hf, Rb, Ta).

The gabbro shows average high values for MgO, FeO_{tot}, Al_2O_3, CaO relative to those for the granite because of its mafic compositions. Granite shows high SiO_2, Na_2O and K_2O values relative to gabbro, reflecting its felsic magma compositions.

4.3 REGRESSION ANALYSIS

Mechanical properties (UCS, Young's modulus, Poisson's ratio) were each plotted as dependent variables against BTS, density, porosity and water content. Statistics results in Table 3.9 for models 1, 2 and 3 represents regression models for UCS, Young's modulus and Poisson's ratio in that order.

The statistical values of rock properties as presented in Table 3.4 show UCS having a large standard deviation relative to the mean. This value could be reflective of the variations in UCS values obtained from the experimental results of standardized and non-standardized specimens and errors in testing protocols. Maximum adherence to standards in specimen preparation and guidelines prior testing is therefore important. The density data for gabbro also exhibits a large standard deviation value. This could be the result of variation in grain sizes of minerals in the respective test specimens. These variations give rise to different porosities and subsequently reflect in the density values. All other properties exhibit small standard deviation values relative to their respective averages. This shows how clustered these datasets are and the level of confidence assigned to them are high in any analysis.

Analysis of variance (ANOVA) as seen in Table 3.5 for model 1 presents the sum of squared errors (SSE), degree of freedom (df), mean square error (MSE), F-test and its significance.

From literature, the R^2 is calculated utilizing equation (26) as:

$$\frac{62319.095}{129767.733} = 0.48$$

An excellent model has R^2 value of 1 which is a measure of the strength of the correlation between the dependent and independent variables. This model is average from its 0.48 R^2 value.

The degree of freedom (df) gives room for a model to assess the strength of the relation between the dependent and independent variables. This influences the R^2, in that as df decreases, R^2 increases. The df for regression is the number of independent variables, in this case 4. The df for residuals is given by the expression:

$$df_r = n - k - 1 \tag{39}$$

where n is the number of observations, k is the number of variables.

Therefore, 15-4-1 = 10 as seen from Table 3.5 is derived from this expression. This value is quite big and has influenced an average 0.48 R^2 of the model. The value 14 for total df of Table 3.7 derived from the expression:

$$df_T = n - 1 \tag{40}$$

The mean square (MS) is defined by the expression:

$$MS = \frac{SS}{df} \tag{41}$$

Where MS is the mean square, SS is the sum of square and df is the degree of freedom. This explains the 15579.774 MS value of the model as derived by dividing 62319.095 / 4. Similarly, the MS of residuals which is 6744.864 is derived from this expression. The MS tells us whether the null hypothesis will be rejected or not through its application in the F-test. The F-test allows the rejection of the null hypothesis at the 0.05 level of significance and is derived by dividing the MS of the model by MS of the residual in the expression:

$$F - test = \frac{MS_{model}}{MS_{residual}} \tag{42}$$

The F-test for model 1 is derived from $\frac{15579.774}{6744.864}$ = 2.310. Its corresponding significance value is indicative of whether the null hypothesis will be rejected or not. This F-test's significance value is 0.129 which must be rejected at the 0.05 significance level. However, in this study, we further analyzed the significance of each independent variable through the t-test at 0.05 significance level.

Similarly, the SSE and SST values from the ANOVA of model 3 from Table 3.6 yields an R^2 value of 0.419. This value is also average and explains the correlation fairly well. The F-test returns 1.803 at 0.205 significance level. This model is further accessed by the significance of the independent variables through the t-test at 0.05 significance level.

Summary correlation coefficients from Table 3.7 indicates UCS has positive correlations with BTS and water content, exhibits inverse correlations with density and porosity. The inverse relation with porosity is comprehensible, considering, a porous rock is susceptible to fractures as the degree of interlocking in its mineral grains are not well sophisticated to respond to applied stress. However, the positive relations shown with BTS and water content, inverse relation with density is problematic especially when analyzing in terms of simple linear relations. This could be the effect of the plurality of the independent variables and the combined effect they wield in predicting the model. The coefficients for BTS and density were not significant at 0.05 p-value, those for porosity and water content were significant. The level of significance will be explained with values from Table 3.9.

Correlation coefficients from Table 3.8 gives a summary of the relations amongst the independent variables for model 3. In this, Poisson's ratio has a positive correlation with density, porosity and water content. It also displays an inverse relation with BTS. All the correlation coefficients for the variables were statistically insignificant, except for density, which was significant at p-value of 0.05.

To investigate the validity of the proposed empirical equations in this study, the t-test was conducted amongst the independent variables using SPSS statistical software package at $p \leq 0.05$. From Table 3.9, the linear regression coefficients derived from model 1 presents -7.817 for BTS, -0.489 for density, -822.517 for porosity and 7573.861 for water content.

The t-value which is a measure of how extreme the calculated coefficients are from the zero mark and how they not likely to be zero as proposed by the null hypothesis is expressed mathematically as:

$$t_i = \frac{b_i}{SE_i} \tag{43}$$

Where t_i is the t value for variable i, b_i is the calculated coefficient of variable i from the model, SE_i is the standard error of variable i.

It implies therefore that, the t-value from Table 3.9 for BTS for model 1, will be given as:

$$\frac{-7.817}{13.905} = -0.562$$

The higher the magnitude of the t-value, the more significant the variable is. In the case of BTS, the t-value is small which affects its significance in the proposed model.

This is explained by the p value obtained for BTS. The p-value is indicative of finding the probability of a sample in the t- distribution curve of BTS which is governed by the values ± 0.562 on the x axis, where the null hypothesis is true. This value returns 0.586 or 58.6% which is very high, hence, BTS is insignificant in the proposed model.

It is observed that, the t-value for density is also low, hence not significant at 0.05 p-value. Porosity and water content, however, show quite high t-values of -2.612 and -2.665 respectively. These values are reflective in their corresponding 0.026 and 0.024 p-values which are statistically significant at the 5% level. The empirical equation for model 1 (UCS), modified from equation (33) will therefore be presented as:

$$UCS = 1770.5 + 7573.8_{water\ content} - 822.5_{porosity} \tag{44}$$

In model 2, from Table 3.9, the p-value for the independent variables return values above the 0.05 significant level. This implies that, the linear coefficients of the variables are more likely to be zero as proposed by the null hypothesis. In this case, we reject the model all together.

It is observed that, all the independent variables from model 3 have p-values higher than the statistically significant 0.05 value apart from density which has a value of 0.032. The empirical equation for this model will therefore involve only one variable as presented below:

$$Poisson'sratio = 0.00104 + 0.0001_{density} \tag{45}$$

In Table 3.10, the statistical results of regression for the granite is presented. It was observed that the p-values of all the independent variables in the 3 models were statistically insignificant at the 0.05 value. The smaller number of samples in this analysis could have influenced this. This meant that empirical equations could not be developed, and the models were rejected.

4.4 ARTIFICIAL NEURAL NETWORK

The network architecture as presented in figure 3.10 shows the input layer, the 2 hidden layers and the output layer. This was generated after saving a desired network script using the simulink interface in matlab.

Table 3.13 shows the performance prediction indices of root mean square error (RMSE), variance accounted for (VAF) and R^2 of the outputs generated by the ANN models. RMSE, VAF and R^2 values were derived from computations from data in Table 3.12 utilizing equations (32), (31) and (26) respectively. Four models were generated and the summation of the ratings of the performance indices for training and testing data for the outputs of a model was computed. The high performance for the training data sets shows good learning of the prediction model while that for the testing data sets indicates good generalization ability of the models. Sometimes, coefficient of correlation of the training data set of a model may be higher while that of the testing data set of the same model may be lower, this necessitated the ratings and rankings concept to determine the best prediction model. The training and testing data are derived from the target output of each model.

The ratings were done such that, a scale from 1 to 5 was formulated with 1 representing the least performer, increasing in that order for the performance prediction indices of the training and testing outputs of the models. A zero rating was however, assigned to performance indices where the values were considered unacceptable. From literature, an RMSE of 0, VAF of 100 and R^2 of 1 represent an excellent model. A VAF or R^2 value returning a negative value was considered outrageous and assigned a zero rating. These benchmarks provided guidelines in the ratings of the outputs.

From Table 3.13 Poisson's ratio training output shows 0.017, 0.0120, 0.0007, 0.0122 RMSE values for models 1,2,3 and 4 in that order. The ratings assigned these RMSE values are 1, 3, 4, 2 in that order considering a value closer to zero represents an excellent model. Similarly, the Poisson's ratio training output shows -58.29, -69.67, 99.73, -21.045 VAF values for models 1,2,3 and 4 in that order. The ratings assigned these values taking into consideration 100 represents an excellent model and a negative value unacceptable are 0, 0, 4, 0, 0 in that order. Also, the R^2 for Poisson's ratio training outputs show -0.098,

0.63, 0.99, 0.54 for models 1, 2, 3 and 4 in that order. Considering a value 1, as an excellent model and a negative value unaccepted, the ratings assigned these R^2 values are 0, 3, 4, 2, in that order.

The rank values are derived from the summation of ratings of the performance indices for each model's training and testing output and a total computed for the overall performance of the model. As seen from the Table 3.13, the value 33 for model 1, is the summation for performance indices of training and test data for UCS, Young's modulus and Poisson's ratio. This value represents the overall performance index for the model. It is clear from these values that, model 2 presents the best performance prediction index with a total rank value of 77, followed by model 3 with 60, model 1 with 33 and model 4 with 19 in that order. Applying this neural network architecture for UCS, Young's modulus and Poisson's ratio prediction, model 2 is the best predictor.

Figures (3.11-3.14) show the regression charts for the models. These present the training, validation, test and overall regression line of best fit. In figure 3.12, the value 0.97702 for the overall coefficient of regression (R) of the model indicates how well it explains the outputs. The error histogram in figures (3.15-3.18) show the distribution of the errors in the models. In figure 3.16, the error histogram for model 2 shows how in nearly 40 instances, the errors generated are near the zero line, making it the best model.

5. CONCLUSION AND RECOMMENDATION

In this work, samples of common igneous rock types, gabbro and granite were studied for petrographic and chemical composition. The essential petrographic parameters influencing strength was the varying grain sizes and the degree of interlocking between the constituent mineral grains. Investigations also, of mechanical and physical properties of 25 specimens of the two rocks was carried out. This revealed very wide variations in UCS of standardized and non-standardized specimens which meant that Young's modulus and Poisson's ratio of some specimens were not measured.

Multiple linear regression analysis of four independent variables (BTS, density, porosity and water content) were employed to predict separately UCS, Young's modulus and Poisson's ratio. Problems arose in the formulation of the models with respect of the independent variables. For example, the empirical relation between UCS and the independent variables was limited to porosity and water content, that for Young's modulus was insignificant and the relation was limited to density with regards Poisson's ratio. One of the important causes of the problem stems from the input parameters especially for UCS data where wide variations were observed. Also, number of datasets employed in the analysis (15 for gabbro and 10 for granite) were not sufficiently large to predict strong and meaningful relations involving all the independent variables. Due to this, the development of non-linear multivariable prediction models with ANN had to be utilized.

In the development of the ANN models, 4 randomly selected datasets for training, testing and validation were used. A model selection procedure based on ranking proposed by (Zorlu et al., 2008) was utilized in selecting the most appropriate dataset providing the best prediction capacity. It was evident that the ANN model has a higher prediction capacity than the multiple regression due to its ability to adapt multiple nonlinearities for interactions between dependent and independent variables, a good generalization capacity and the ability to cope with missing data. However, both models are significant statistically and can be used for practical purposes.

It is concluded that the developed ANN prediction model 2 is best, and can be used for inferring the UCS, Young's modulus and Poisson's ratio of the two igneous rock types for rock mechanics and or engineering purposes. The regression models are, however, open for more development with large datasets.

The findings from this study recommend adherence to standard procedure from sample preparation (in rock mechanical tests) through to the conduct of tests. This was evident in the wide variation in UCS test data between standardized and non-standardized samples. It is also recommended that for reliability in model prediction, datasets should be large to give meaningful generalization between independent and dependent variables.

6. SUMMARY

This thesis work is about the characterization of some selected rock properties and comparing predictive models of ANN and regression techniques. In the utilization of rocks in engineering, rock strength is an essential parameter with regards stability of the structures and uniaxial compressive strength (UCS) is one index property relied on, by engineers. Predictive models of UCS, Young's modulus and Poisson's ratio were developed from datasets comprising BTS, density, porosity and water content of gabbro and granite from Otamänki area, central Finland.

Sampling was done at two rock quarry sites at Vuorokas and Pikkukallio in the Otamänki area of central Finland where boulders of the two rock types were obtained for further processing at the Oulu Mining School. Obtaining core samples was very challenging, as we relied on handheld drilling machines for the purpose. This translated in the limited core samples for the tests and an even greater problem of some cores not having parallel and smooth edges. Sample preparations and tests procedures for the selected rock properties in this work were carried out following standard methods. Some cylindrical cores for UCS test, however, did not meet test standards but tests were carried out regardless to observe variations.

Test results representing mechanical and physical properties, petrological and chemical compositions of the two rock types were obtained. Regression and ANN analysis were run with dataset from the mechanical and physical properties from 15 gabbro and 10 granite specimens. The mean and mode for the dataset representing Young's modulus and Poisson's ratio respectively, were used to complement for the unavailable of data for non-standardized specimens.

Multiple regression using SPSS software with UCS, Young's modulus and Poisson's ratio separately as dependent and BTS, density, porosity and water content as independent variables was conducted. The analysis showed strong correlations amongst the various variables, but correlation coefficients were deemed statistically significant with the t-test at p-value ≤ 0.05. With this, the empirical equation representing the correlations between the dependent and independent variables was limited to porosity and water content for

UCS, was insignificant with regards Young's modulus and limited to density for Poisson's ratio. These are outlined in equations (44) and (45).

Prediction with ANN was done using Matlab 2019a software. Multivariable prediction consisting of BTS, density, porosity and water content as inputs, two hidden layers with 14 neurons in the first layer and 3 neurons in the second layer and UCS, Young's modulus and Poisson's ratio as outputs. The data for this analysis was sampled from 70% of the datasets using Levenberg-Marquardt algorithm (trainlm). The training was stopped when the mean squared error (MSE) was observed to be relatively small. Four models were generated, the root mean square error (RMSE), variance accounted for (VAF) and R^2, representing performance prediction indices were used in rating and ranking the models for selection of the best model.

The essential petrographic parameters affecting strength in this work was the varying grain sizes which reflected in the degree of interlocking of the grains. Models generated from both regression and ANN were statistically good, but that for ANN was more reliable because of its non-linearity and good generalization capability. Fallouts from this work recommend adherence to testing standards and protocols, and the use of large dataset to enhance reliable prediction of complex. 'property' behaviour of systems.

7. REFERENCES

Abbaszadeh, M., Hezarkhani, A., Soltani-Mohammadi, S., 2016. Proposing drilling locations based on the 3D modeling results of fluid inclusion data using the support vector regression method, J. Geochem. Explor. 165 23–34.

Abdulraheem, A., Ahmed, M., Vantala, A., Parvez, T., 2009. "Prediction rock mechanical parameters for hydrocarbon reservoirs using different artificial intelligence techniques," SPE Paper126094, 2009

Abe, S., 2008. Support Vector Machines for Pattern Classification, Springer-Verlag London Limited,350 pp.

Abu-Kiefa, M. A., 1998. General regression neural networks for driven piles in cohesionless soils. J. Geotech. Geoenv. Engrg., ASCE, Vol.123, No.12, (December 1998), pp. 1177–1185, ISSN 1090-0241

Aladejare, A.E., 2016. Development of Bayesian probabilistic approaches for rock property characterization. Ph.D. thesis, City University of Hong Kong, Hong Kong

Aladejare, A.E., 2019.Evaluation of empirical estimation of uniaxial compressive strength of rock from measurements of index and physical tests. J Rock Mech Geotech Eng (Accepted)

Aladejare, A.E., Wang, Y., 2019b.Estimation of rock mass deformation modulus using indirect information from multiple sources. Tunn Undergr Space Technol 85:76–83

Aladejare, A.E., Wang, Y., 2017a. Evaluation of rock property variability. Georisk: Assessment and Management of Risk for Engineered Systems and Geohazards 11 (1): 22-41

Aladejare A.E., Wang, Y., 2019a. Probabilistic characterization of Hoek–Brown constant mi of rock using Hoek's guideline chart, regression model and uniaxial compression test. Geotech Geol Eng 1–16

Aladejare, A.E., Wang, Y., 2017b. Sources of uncertainty in site characterization and their impact on geotechnical reliability-based design. ASCE-ASME J Risk Uncertain Eng Syst Part A Civ Eng 3(4):04017024

Al-Shayea, N. A., 2004. "Effects of testing methods and conditions on the elastic properties of limestone rock," *Engineering Geology*, vol. 74, no. 1-2, pp. 139–156.

Alvarez Grima, M., Babuska, R., 1999. Fuzzy model for the prediction of unconfined compressive strength of rock samples. International Journal of Rock Mechanics and Mining Sciences 36 (3), 339–349

Arbib, M. A., 1995 *The Handbook* of *Brain Theory and Neural Networks* (Cambridge, MA: Bradford Books MIT Press)

Artun, E., Mohaghegh, S., Toro, J., Wilson, T., Sanchez, A., 2005. Reservoir characterization using intelligent seismic inversion, in: SPE Eastern Regional Meeting Held in Morgantown, SPE 98012.

ASTM. 2008a. Designation: D4543-08: Standard Practices for Preparing rock core as cylindrical test specimens and verifying conformance to dimensional and shape tolerances, ASTM International, West Conshohocken, PA.

ASTM. 2008b. Designation D3967-08: Standard Test Method for Splitting Tensile Strength of Intact
Rock Core Specimens. ASTM International, West Conshohocken, PA.

ASTM. 2010. Designation D2216-10: Standard Test Methods for Laboratory Determination of Water
(Moisture) Content of Soil and Rock by Mass, ASTM International, West Conshohocken, PA.

ASTM. 2014. Designation: D7012-14: Standard Test Methods for Compressive Strength and Elastic Moduli of Intact Rock Core Specimens under Varying States of Stress and Temperatures, ASTM International, West Conshohocken, PA.

Baecher, G.B., Christian, J.T., 2003. Reliability and statistics in geotechnical engineering. Wiley, Hoboken, p 605p

Baik, K., 2002. Optimum Driving Method for Steel Pipe Piles in Sands, J. of Civil Engineering, Vol.22, No.1-C, pp. 45-55.

Baoping, L., Hongzhi, B., 2005. "Advances in calculation methods for rock mechanics parameters," *Petroleum Drilling Techniques*, vol. 33, no. 5, pp. 44–47.

Baoping, Z., Economides, M.J., 2002. *Reservoir Stimulation*,Petroleum Industry Press, Beijing, China, 3rd edition.

Barton, N., 2002. Some new Q-value correlations to assist site characteristics and tunnel design, Int. J. Rock Mech. Min. Sci. 39 (2002) 185–216.

Basu, A., Celestino, T.B., Bortolucci, A.A., 2009. Evaluation of rock mechanical behaviours underuniaxial compression with reference to assessed weathering grades. Rock Mechanics and RockEngineering 42, 73–93.

Bea, R.G., Jin, Z., Valle, C., Ramos, R., 1999. ''Evaluation of reliability of platform pile foundations.'' J. Geotech. Geoenviron. Eng., ASCE, Vol.125, No.8, (August 1999), pp. 696–704, ISSN 1090-0241

Bery, A.A., Saad, R., 2012. Correlation of seismic P-wave velocities with engineering parameters (N value and rock quality) for tropical environmental study. Int. J. Geosci. 3, 749–757.

Bishop, C. M., 2006. Pattern Recognition and Machine Learning, Springer Science and Business Media, 743 pp.

Bozorgzadeh, N, Escobar, M.D., Harrison, J.P., 2018. Comprehensive statistical analysis of intact rock strength for reliability-based design. International Journal of Rock Mechanics and Mining Sciences 2018a; 106:374e87.

Bozorgzadeh, N, Harrison, J.P., Escobar, M.D., 2018. Hierarchical Bayesian modelling of geotechnical data: application to rock strength. Geotechnique 2018.

Ceryan, N., Okkan, U., Kesimal, A., 2012. Application of generalized regression neural networks in predicting the unconfined compressive strength of carbonate rocks, Rock Mech. Rock Eng. 45 1055–1072.

Chaki, S., Takarli, M., Agbodjan, W.P., 2008. Influence of thermal damage on physical properties of a granite rock: porosity, permeability and ultrasonic wave evolutions. Constr. Build. Mater.22, 1456–1461.

Chang, C., Zoback, M. D., Khaksar, A., 2006. "Empirical relations between rock strength and physical properties in sedimentary rocks," *Journal of Petroleum Science and Engineering*, vol. 51, no.3, pp. 223–237.

Cho, S.E., 2009. Probabilistic stability analyses of slopes using the ANN-based response surface, Computers and Geotechnics, Vol.36, pp. 787–797, ISSN 0266-352X

Contreras, L.F, Brown, E.T, Ruest, M., 2018. Bayesian data analysis to quantify the uncertainty of intact rock strength. Journal of Rock Mechanics and Geotechnical Engineering 2018;10(1):11e31.

Das, S.K., Basudhar, P.K., 2006. Undrained lateral load capacity of piles in clay using artificial neural network, Computers and Geotechnics, Vol.33, pp. 454–459.

Das, S.K., Kumar, A., Das, B., Burnwall, A.P., 2013. On soft computing techniques in various areas. Rupak Bhattacharyya et al. (Eds) : ACER 2013, pp. 59–68, 2013.

Delatte, N., Chen, S., Maini, N., 2002 The application of nondestructive evaluation to subway tunnel systems, in: TRB 2003 Annual Meeting, 2002, pp. 2–8

Duda, R. A., Hart, P. E., Stork, D. G., 2002. Pattern Classification, 2nd edition, Wiley & Son, 680 pp.

Elorant, P., 2004. Forsmark site investigation e drill hole KFM01A: indirect tensile strength test (HUT). SKB P-04-171. Swedish Nuclear Fuel and Waste Management Company (SKB); 2004a.

Elorant, P., 2004. Forsmark site investigation e drill hole KFM01A: triaxial compression test (HUT). SKB P-04-177. SKB; 2004b.
Elorant P. Forsmark site investigation e drill hole KFM01A: uniaxial compression test (HUT). SKB P-04-176. SKB; 2004c.

Fairhurst, C., 2003. Stress estimation in rock: a brief history and review. Int. J. Rock Mech. Min. Sci. 40, 957–973

Ferentinou, M.D., Sakellariou, M.G., 2007. Computational intelligence tools for the prediction of slope performance, Computers and Geotechnics, Vol.34, No.5, pp. 362-384, ISSN 0266-352X

Fjær, E., Holt, R.M., Horsrud, P., Raaen, A. M., Risnes, R., 2008. *Petroleum Related Rock Mechanics*, vol. 53, 2nd edition.

Funatsu, T., Seto, M., Shimada, H., et al., 2004. Combined effects of increasing temperature and confining pressure on the fracture toughness of clay bearing rocks. International Journal of Rock Mechanics & Mining Sciences 41(6): 927-938.

Gholami, R., Moradzadeh, M., Maleki, S.H., Amiri, S., Hanachi, J., 2014. Applications of artificial intelligence methods in prediction of permeability in hydrocarbon reservoirs, J. Pet. Sci. Eng. 122 643–656.

Gercek, H., 2007. Poisson's ratio values for rocks. Int J Rock MechMin Sci 44:1–13. doi: 10.1016/j.ijrmms.2006.04.011

Gokceoglu, C., 2002. A fuzzy triangular chart to predict the uniaxial compressive strength of the Ankara agglomerates from their petrographic composition.Engineering Geology 66, 39–51.

Gokceoglu, C., Zorlu, K., 2004. A fuzzy model to predict the uniaxial compressive strength and modulus of elasticity of a problematic rock. Engineering Applications of Artificial Intelligence 17, 61–72.

Goh, A.T.C., Kulhawy, F.H., Chua, C.G., 2005. Bayesian neural network analysis of undrained side resistance of drilled shafts, Journal of Geotechnical and Geoenvironmental Engineering, Vol.131, No.1, pp. 84-93.

Gorski, B, Conlon, B., 2007. Forsmark site investigation: determination of the direct and indirect tensile strength on cores from borehole KFM01D. SKB P-07-76. SKB.

Guo, J., Liu, Y., 2014. "A comprehensive model for simulating fracturing fluid leak off in natural fractures," *Journal of Natural Gas Science and Engineering*, vol. 21, pp. 9770–985.

Haykin, S., 1999. Neural networks – a comprehensive foundation. London: Pearson.

Hoek, E, Carranza-Torres, C, Corkum, B., 2002. HoekeBrown failure criterion e 2002 edition. In: NARMS-TAC 2002: Mining and Tunnelling Innovation and Opportunity, Proceedings of the 5th North American Rock Mechanics Symposium and the 17th Tunnelling Association of Canada Conference (NARMS-TAC 2002), vol. 1. Toronto, Canada: University of Toronto Press; 2002. p. 267e73.

Hu, D.W., Zhang, F., Shao, J.F., Gatmiri, B., 2014. Influences of Mineralogy and Water Content on theMechanical Properties of Argillite. Rock Mechanics and Rock Engineering 47:157–166. DOI 10.1007/s00603-013-0413-8.

Hudson, J.A., 1992. Rock properties, testing methods and site characterization. In: Hudson, J.A. (Ed.), In: Rock Engineering—Principle, Practice & Projects, vol. 1. Pergamon, Oxford, UK, pp. 1–39.

Hudson, J.A., 1993. Rock properties, testing methods and site characterization. In: Hudson, J.A. (Ed.), In: Rock Engineering—Principle, Practice & Projects, vol. 2. Pergamon, Oxford, UK, pp. 1–39.

Hudson, J.A., 1995. Rock properties, testing methods and site characterization. In: Hudson, J.A. (Ed.), In: Rock Engineering—Principle, Practice & Projects, vol. 3. Pergamon, Oxford, UK, pp. 1–39.

Hudson, J.A., 2012. Design methodology for the safety of underground rock engineering. J. Rock Mech. Geotech. Eng. 4 (3), 205–214

Hudson J. A., Crouch S. L. and Fairhurst C., 1972. Soft, stiff and servo-controlled testing machines: a review with reference to rock failure. Eng. Geo/. (Amsterdam) 6, 155-189 (1972)

Hudson, J.A., Harrison, J.P., 1997. Rock Engineering Mechanics- An Introduction to the Principles. Elsevier, Oxford

Ibrahim, D., 2016. An overview of soft computing. 12th International Conference on Application of Fuzzy Systems and Soft Computing, ICAFS 2016, 29-30 August 2016, Vienna, Austria. Procedia Computer Science 102 (2016) 34 – 38

Jackson, K., Kingman, S.W., Whittles, D.N., et al., 2008. The effect of strain rate on the breakage behavior of rock. Archives of Mining Sciences 53(1): 3-22.

Jacobsson, L., 2004a. Forsmark site investigation e borehole KFM01A: triaxial compression test of intact rock. SKB P-04-227. SKB.

Jacobsson, L., 2004b. Forsmark site investigation e borehole KFM01A: uniaxial compression test of intact rock. SKB P-04-223. SKB.

Jacobsson, L., 2004c. Forsmark site investigation e drill hole KFM01A: indirect tensile strength test. SKB P-04-170. SKB.

Jacobsson, L., 2006. Forsmark site investigation e borehole KFM01D: triaxial compression test of intact rock. SKB P-06-214. SKB.

Jacobsson, L., 2007. Forsmark site investigation e boreholes KFM01A and KFM02B: micro crack volume measurements and triaxial compression tests on intact rock. SKB P-07-93. SKB.

Jeong, H.S., Kang, S.S., Obara, Y., 2007. Influence of surrounding environments and strain rates on the strength of rocks subjected to uniaxial compression. International Journal of Rock Mechanics & Mining Sciences 44(3): 321-331.

Jin, L. H. Y., Meng, Q., Ma, D., Han G., Gao, F., Wang, S., 2018. Experimental investigation of the mechanical behaviors of grouted sand with uf-oa grouts. MDPI, 13

Juang, C.H., Chen, C.J., 1999. CPT-based liquefaction evaluation using artificial neural networks, Computer-Aided Civil and Infrastructure Engineering, 14(3), 221-229.

Kahraman, S., 1999. Rotary and percussive drilling prediction using regression analysis. Int. J. Rock Mech. Min. Sci 1999; 36:981–9.

Kahraman, S., Altun, H., Tezekici, B.S., Fener, M., 2006. Sawability prediction of carbonate rocks from shear strength parameters using artificial neural networks. International Journal of Rock Mechanics and Mining Sciences 43,157–164.

Karakus, M, Kumral, M, Kilic, O., 2005. Predicting elastic properties of intact rocks from index tests using multiple regression modelling. Int. J. Rock Mech. Min. Sci 2005; 42:323–30.

Katz, O, Reches, Z, Roegiers J.C., 2000. Evaluation of mechanical rock properties using a Schmidt hammer. Int. J. Rock Mech. Min. Sci 2000; 37:723–8.

Kodama, J.; Goto, T.; Fujii, Y.; Hagan, P., 2013. The effects of water content, temperature and loading rate onstrength and failure process of frozen rocks. Int. J. Rock Mech. Min. Sci. 2013, 62, 1–13.

Komurlu, E., 2018. Loading rate conditions and specimen size effect on strength and deformability of rock materials under uniaxial compression. *Geo-Engineering* **9,** 17 (2018). https://doi.org/10.1186/s40703-018-0085-z

Langford, J.C., Diederichs, M.S., 2015. Quantifying uncertainty in HoekeBrown intact strength envelopes. International Journal of Rock Mechanics and Mining Sciences 2015; 74:91e102.

Lewis, W. E., Tandanand, S., 1974 (Ed.) United States Department of the Interior, Bureau of Mines (USBM) Bureau of Mines Test Procedures for Rocks. Information Circular 8628.

Liang, C.Y., Zhang, Q.B., Li, X., et al., 2015. The effect of specimen shape and strain rate on uniaxial compressive behavior of rock material. Bulletin of Engineering Geology & the Environment: 1-13.

Liu, S., Xu, J.Y., 2015. An experimental study on the physic-mechanical properties of two post-high-temperature rocks. Engineering Geology 185(2): 63-70.

Locatelli, L., Di Marco, G., Zanichelli, C., Jarre, P., 2001. Rehabilitation of highway tunnels-techniques and procedures, in: A.I.T.E.S-ITA 2001 World Tunnel Congress, 2001, pp. 1–3.

Manouchehrian, A., Sharifzadeh, M., Hamidzadeh, M. R., Nouri, T., 2013. Selection of regression models for predicting strength and deformability properties of rocks using GA. International Journal of Mining Science and Technology 23 (2013) 495–501

Martinez-Ramon, M., Cristodoulou, C., 2006.Support Vector Machines for Antenna Array Processing and Electromagnetic, Morgan& Claypool,126 pp.

McCombie, P, Wilkinson, P., 2002. The use of the simple genetic algorithm in finding the critical factor of safety in slope stability analysis. Comput Geotech 2002; 29:699–714

Mavko, G., Mukerji, T., Dvorkin, J., 2009. *The Rock Physics Handbook: Tools for Seismic Analysis in Porous Media*, Cambridge University Press, Cambridge, UK, 2nd edition.

Meng, Z, Peng, S, Fu, J., 2002. Key factors to control rock mechanical properties in coal measure formations. Chinese J Rock Mech Eng. 21(1):102-106 (in Chinese)

Miskovsky, K., Tabora, D.M., Kou, S.Q., Lindqvist, P.A., 2004. Influence of the mineralogical composition and textural properties on the quality of coarse aggregates. J. Mater. Eng. Perform. 2004, 13, 144–150.

Najjar, Y.M., Ali, H.E., 1999. On the use of neuronets for simulating the stress–strain behavior of soils, 7th International symposium on numerical models in geomechanics, pp. 657–662, Austria.

Nasseri, M.H.B., Tatone, B.S.A., Grasselli, G., et al., 2009. Fracture Toughness and Fracture Roughness Interrelationship in Thermally treated Westerly Granite. Pure & Applied Geophysics 166(5): 801-822.

Nefeslioglu, H.A., Gokceoglu, C., Sonmez, H., 2003. A Mamdani model to predict the weighted joint density. Lecture Notes in Artificial Intelligence 2773, 1052–1057.

Nefeslioglu, H.A., Gokceoglu, C., Sonmez, H., 2006. Indirect determination of weighted joint density (wJd) by empirical and fuzzy models: Supren (Eskisehir, Turkey) marbles. Engineering Geology 85, 251–269.

Neaupane, K.M., Achet, S.H., 2004. Use of backpropagation neural network for landslide monitoring: a case study in the higher Himalaya, Engineering Geology, Vol.74, pp. 213–226

Negnevitsky, M., 2002. Artificial Intelligence: A Guide to Intelligent Systems. Addison-Wesley, England.

Örztutk, N., 2003. Use of genetic algorithm to design optimal neural network structure, Engineering Computations, Vol.20, No.8, pp. 979-997

Ozer, M., Isik, N.S., Orhan, M., 2008. Statistical and neural network assessment of the compression index of clay-bearing soils, Bull Eng Geol Environ, Vol.67, pp. 537–545

Ozguven, A., Ozcelik, Y., 2014. Effects of high temperature on physico-mechanical properties of Turkish natural building stones. Engineering Geology 183: 127-136.

Park, H.I., Cho, C.H., 2010. Neural Network Model for Predicting the Resistance of Driven Piles Marine Geosources and Geotechnology, In Press

Park, H.I., Keon, G.C., Lee, S.R., 2009. Prediction of Resilient Modulus of Granular Subgrade Soils and Subbase Materials Based on Artificial Neural Network, Road Materials and Pavement Design, Vol.10, No. 3, pp. 647- 665.

Park, H.I., Kim, Y.T., 2010. Prediction of Strength of Reinforced Lightweight Soil Using an Artificial Neural Network, Engineering Computation, In press

Park, H.I.,Lee, S.R., 2010. Evaluation of the compression index of soils using an artificial neural network Computers and Geotechnics, Submitted.

Park, H. I., 2011. Study for Application of Artificial Neural Networks in Geotechnical Problems.

Phoon, K.K., Kulhawy, F.H., 1999. Characterization of geotechnical variability. Can Geotech J 36(4):612–624

Priest, S., D., 1993. Discontinuity Analysis for Rock Engineering, p. 473. Chapman & Hall, London.

Prikryl, R., 2006. Assessment of rock geomechanical quality by quantitative rock fabric coefficients: limitations and possible source of misinterpretations. Engineering Geology, 87, 149- 162.

Prikryl, R., Melounova, L., Varilova, Z., Weishauptova, Z., 2007.Spatial relationships of salt distribution and related physical changes of underlying rocks on naturally weathered sandstone exposures (Bohemian Switzerland National Park, Czech Republic).Environmental Geology 52, 409–420.

Qi, C.Z., Wang, M.Y., Qian, Q.H., 2009. Strain-rate effects on the strength and fragmentation size of rocks. International Journal of Impact Engineering 36(12): 1355-1364.

Ranjbar-Karami, R., kadkhodaie-Ilkhchi, A., Shiri, M., 2014. "A modified fuzzy inference system for estimation of the static rock elastic properties: a case study from the Kangan and Dalan gas reservoirs, South Pars gas field, the Persian Gulf," *Journal of Natural Gas Science and Engineering*, vol. 21, pp. 962–976.

Rocchi, V., Sammonds, P.R., Kilburn, C.R.J., 2002. Flow and fracture maps for basaltic rock deformation at high temperatures. Journal of Volcanology and Geothermal Research 120: 25-42.

Sheinin, V.I., Blokhin, D.I., 2012. Features of thermomechanical effects in rock salt samples under uniaxial compression. Journal of Mining Science 48(1): 39-45.

Shi, J.J.,2000. Reducing prediciton error by transforming input data for neural networks, Journal of Computing in Civil Engineering, Vol.14, No.2, pp. 109-116.

Singh, V.K., Singh, D., Singh, T.N., 2001. Prediction of strength properties of some schistose rocks from petrographic properties using artificial neural Networks. International Journal of Rock Mechanics and Mining Sciences 38 (2), 269–284.
Smith, M.R., Collis, L., 2001. Aggregates: Sand, Gravel and Crushed Rock Aggregates for Construction Purposes; Spec.Publ. 17; The Geological Society: London, UK, 2001.

Sonmez, H., Gokceoglu, C., Nefeslioglu, H.A., Kayabasi, A., 2006. Estimation of rockmodulus: For intact rock with an artificial neural network and for rock masses with a new empirical equation. International Journal of Rock Mechanics and Mining Sciences 43, 224–235.

Stephansson, O., Zang, A., 2012. ISRM suggested methods for rock stress estimation—part 5: establishing a model for the in-situ stress at a given site. Rock Mech. Rock. Eng. 45, 955–969.

Tug˘rul, A., 2004. The effect of weathering on pore geometry and compressive strength of selected rock types from Turkey. Eng. Geol. 75, 215–227.

Ulusay, R., 2014. The ISRM suggested methods for rock characterization, testing and monitoring: 2007-2014. ISBN 978-3-319-07713-0 (eBook) Springer Cham Heidelberg New York Dordrecht London

Ulusay, R., Hudson, J.A., 2007. The complete ISRM suggested methods for rock characterisation, testing and monitoring: 1974e2006. International Society for Rock Mechanics and Rock Engineering; 2007.

Watkins, H., Bond, C.E., Healy, D., Butler, R.W.H., 2015. Appraisal of fracture sampling methodsand a new workflow to characterise heterogeneous fracture networks at outcrop. J. Struct. Geol.72, 67–82.

Xu, G.M.; Liu, Q.; Peng, W.; Chang, X., 2006. Experimental study on basic mechanical behaviors of rocks under lowtemperatures. Chin. J. Rock Mech. Eng. 2006, 25, 2502–250.

Yavuz, H., Demirdag, S., Caran, S., 2010. Thermal effect on the physical properties of carbonate rocks. Int. J. Rock Mech. Min. Sci. 47, 94–103.

Yesiloglu-Gultekin, N., Gokceoglu, C., Sezer, E. A., 2013. Prediction of uniaxial compressive strength of granitic rocks by various nonlinear tools and comparison of their performances, Int. J. Rock Mech. Min. Sci. 62 113–122.

Yilmaz, I, Yuksek G., 2009. Prediction of the strength and elasticity modulus ofgypsum using multiple regression, ANN, and ANFIS models. Int J Rock Mech Min Sci 2009; 46:803–10.

Yilmaz, I., 2010.Influence of water content on the strength and deformability of gypsum. Int. J. Rock Mech. Min. Sci.,47, 342–347.

Yoo, C., Kim, J.M., 2007. Tunneling performance prediction using an integrated GIS and neural network, Computers and Geotechnics, Vol.34, pp. 19-30, ISSN 0266-352X

Yuming, S., Guowei, L., 2000. “Experimental study on dynamic and static parameters of rocks under formation conditions,” *Journal of Chengdu College Geology of Technology*, vol. 27, no. 3, pp. 249–255

Zhang, A., Stephansson, O., 2010. Stress Field of the Earth’s Crust. Springer Science and BusinessMedia BV, Dordrecht.

Zhang, J.; Deng, H.; Taheri, A., 2018. Degradation of physical and mechanical properties of sandstone subjected tofreeze-thaw cycles and chemical erosion. Cold Reg. Sci. Technol. 2018, 155, 37–46.

Zhang, J.; Deng, H.; Taheri, A., 2019. Deterioration and strain energy development of sandstones under quasi-static and dynamic loading after freeze-thaw cycles. Cold Reg. Sci. Technol. 2019, 160, 252–264.

Zhang, L., 2004. Drilled Shafts in Rock—Analysis and Design. Balkema, Leiden.

Zhang, L., Einstein, H.H., 2010. The planar shape of rock joints. Rock Mech. Rock. Eng. 43, 55–68.

Zhao, H.B., 2007. Slope reliability analysis using a support vector machine, Computers and Geotechnics, in press.

Zoback, M. D., 2007.Reservoir Geomechanics, Cambridge University Press, US, 450 p.